ULTRA-BROADBAND PHASE-MATCHING ULTRASHORT-LASER-PULSE MEASUREMENT TECHNIQUES

A Dissertation
Presented to
The Academic Faculty

by

DONGJOO LEE

In Partial Fulfillment
of the Requirements for the Degree
Doctor of Philosophy

Georgia Institute of Technology
August 2007

ULTRA-BROADBAND PHASE-MATCHING ULTRASHORT-LASER-PULSE MEASUREMENT TECHNIQUES

Approved by:

Dr. Rick Trebino, Advisor
School of Physics
Georgia Institute of Technology

Dr. Ali Adibi
School of Electrical and Computer Engineering
Georgia Institute of Technology

Dr. John Buck
School of Electronocal and computer engineering
Georgia Institute of Technology

Dr. Philip First
School of Physics
Georgia Institute of Technology

Dr. Chandra Raman
School of Physics
Georgia Institute of Technology

Date Approved: [August 4, 2007]

Dedicated to my wife, Seonghee Jeong, and my parents

ACKNOWLEDGEMENTS

I wish to thank all people who helped me in many different ways during my graduate school years. First of all, I would like to especially thank Rick Trebino not only for sharing his knowledge and experience since the beginning, but also for his constantly encouraging and motivating me, which could make this thesis possible. In addition, I thank Aparna, Erick, Lina, Mark, Neeraj, Pablo, Pam, Qiang, Saman, Selcuk, Xuan, Xun, and Zyiang but I want to especially thank Pablo for discussing many problems and helping me with pleasure. And I would like to especially thank Qiang and Selcuk for helping me in many ways during my first and second years in this group. Finally, I wish to thank to my family: my father Eunsoo, my mother Soonduck Kim, my sisters Haegyung, Gyunghee, and my brother Chunjoo and especially thank my wife Seonghee Jeong and my son Seungmin.

TABLE OF CONTENTS

LIST OF FIGURES

LIST OF ABBREVIATIONS

Abbrev1	FROG	Frequency-Resolved-Optical Gating
Abbrev2	SHG	second-harmonic generation
Abbrev3	BBO	beta-barium borate
Abbrev4	PG	polarization-gate
Abbrev5	SD	self-diffraction
Abbrev6	TG	transient-grating
Abbrev7	SPIDER	spectral phase interferometry for direct electric-field reconstruction
Abbrev8	GRENOUILLE	Grating-Eliminated No-nonsense Observation of Ultrafast Laser-Light E-Field
Abbrev9	SC	supercontinuum
Abbrev10	PCF	crystal fibers
Abbrev11	SEM	scanning electron microscope
Abbrev12	GVD	Group velocity dispersion
Abbrev13	MFD	mode field diameter
Abbrev14	X FROG	cross-correlation frequency resolved optical gating
Abbrev15	SFG	sum frequency generation
Abbrev16	FWHM	Full-width-half-maximum
Abbrev17	TG X FROG	transient-grating cross-correlation frequency-resolved-optical-gating
Abbrev18	NA	numerical aperture
Abbrev19	FFT	Fast Fourier-transform
Abbrev20	IFFT	inverse Fast-Fourier-transform
Abbrev21	CPA	chirped-pulse-amplifiers
Abbrev22	OPA	optical parametric amplifier

SUMMARY

In the past several decades the technology for the creation and use of ultrashort pulses has progressed tremendously. In addition, the means of measuring these pulses has progressed so rapidly. However, despite recent great advances in ultrashort-pulse measurement techniques, much remains to be done. In particular, pulse-measurement devices have relatively small wavelength-tuning ranges, and the phase-match is problematic for the pulses with a wide bandwidth such as supercontinuum. This is mainly because most of pulse measurement devices are based on the second-harmonic-generation process. In the thesis, we propose new pulse measurement techniques which can overcome these problems. In addition, in chapter 4, we show a very simplified version of TG FROG which can measure a very broadband of wavelengths, ranging from the UV to the IR.

CHAPTER 1

INTRODUCTION

In the past several decades the technology for the creation and use of ultrashort pulses has progressed tremendously. Now, it is possible to generate laser pulses as short as a few femtoseconds in duration, and such pulses have been used for a wide range of applications. In addition, the methods of measuring these pulses have progressed so rapidly. In the early 1990s, there were tremendous improvements in the field of ultrashort pulse measurements and various schemes, which could characterize temporal behavior of ultrashort pulses, had been presented. It is no doubt that the most significant one of these schemes is Frequency-Resolved Optical Gating (FROG) [1, 2, 3].

FROG is the first self-referencing pulse measurement device that can extract the intensity and phase information of the pulse. Simply, FROG is a spectrally resolved autocorrelation, and so nonlinear-optical processes that can be used for making autocorrelators can used to make FROG geometries [4, 5]. Depending on the nonlinear optical processes, we can have five FROG geometries. Four of them, such as polarization gate, and self-diffraction, and transient grating, and third-harmonic-generation FROG geometries use the third-order nonlinearity, while one of them, second-harmonic-generation FROG geometry, uses the second-order nonlinearity. Each of the FROG geometries has its own disadvantages and advantages. Therefore, it is necessary to choose the right one, depending on what they have. However, it was true that ignoring the pulse measurement techniques based on the third-order nonlinear process, we have focused on the pulse measurement techniques based on the second-order process, not only for FROG

geometries but also other pulse measurement techniques. This was mainly because the pulse energy, which most of ultrafast research groups could have, was not strong enough to generate signals from third-order nonlinear crystal. However, in these days, many high power ultrashort-laser sources, which many research groups have, are accessible, and the pulses from the sources need to be characterized.

A significant improvement in the ultrashort-laser-pulse measurement field was the advent of the simplified version of FROG. O'Shea et al. demonstrated an arrangement of FROG which could be tremendously simplified using a Fresnel biprism, which replaced the beam splitter and delay line, and a thick second-harmonic crystal, which replaced the thin crystal and spectrometer in the FROG. We call the device GRENOUILLE, a relative of FROG [7, 8, 9]. The invention of GRENOUILLE makes an impact on the ultrafast-laser-pulse measurement field as well as the other application fields, such as chemistry-molecular vibrations and re-orientation, and engineering, of the ultrafast-laser-pulse because now they can measure their pulses easily even though they are not good at optics or laser.

Now, it is possible to generate ultrafast-laser-pulses with a very broad bandwidth. An example is continuum from bulk materials or from microstructure fibers. An application of generating continuum is making the pulse much shorter because in order to generate very short pulses, we need to generate pulses with enough bandwidth first and we need to compress the pulse. Also, there are numerous far-reaching applications for the continuum. Therefore, generating and understanding broadband continuum has been a subject of intensive research since supercontinuum generation from the microstructure fibers and the tapered fibers.

When trying to measure the broadband pulse, the phase-matching condition is problematic because even extremely thin second-harmonic crystal can phase-match several hundreds nm at most. In this thesis, after briefly mentioning the basic stuffs about the FROG, we propose two solutions for broadband phase-matching condition, and we demonstrate two arrangements which can phase-match the supercontinuum pulses.

In addition, the devices, based on SHG process, have relatively small wavelength-tuning ranges due to a relatively stringent phase-matching requirement. Therefore, if we have several ultrafast-laser sources or if we have an ultrafast-laser source with a great tenability, such as an optical parametric amplifier/oscillator, we need to build (or buy) several pulse measurement devices. Also, the devices, based on SHG process, have a limited wavelength range and cannot operate in the UV. It necessitates another pulse measurement device using third-order nonlinearity instead. The next part of this these is dedicated to developing a device which can measure pulses with a different center wavelengths, ranging from the UV to the IR, with no change of optics. In addition to this, like GRENOUILLE, this device is simplified tremendously.

1.1 THE INTENSITY AUTOCORRELATION

Historically, an attempt to measure the ultrashort pulse's electric field is the intensity autocorrelation. Figure 1 shows the experiment layout for an intensity autocorrelator using second-harmonic generation (SHG) which can measure an unknown pulse's intensity in the time domain. The unknown pulse is split into two replicas by a beam splitter, and spatially overlapping the two replicas in an instantaneously responding nonlinear-optical medium, such as a beta-barium borate (BBO) crystal, a SHG crystal. One of two replicas is variably delayed with respect to the other by a translation stage. A SHG crystal produces electric field, a product of the electric fields of the two replicas, at twice the frequency of the unknown pulse. An intensity of the electric field is proportional to the product of the intensities of the two pulses:

$$I_{sig}^{SHG}(t,\tau) \propto I(t)I(t-\tau)$$

where I(t) is the pulse intensity and τ is the delay between the two replicated pulses. Since detectors are too slow to time-resolve the signal, the measurement produces the time integral:

$$A^{(2)}(\tau) = \int_{-\infty}^{\infty} I(t)I(t-\tau)dt$$

Above equation is the definition of the intensity autocorrelation, or simply the autocorrelation: we abbreviate it as the autocorrelation, if there is no confusion with the field autocorrelation. An autocorrelation yields a measurement of the unknown pulse's duration, because there is no second harmonic intensity if the pulses do not overlap in time. In other word, the intensity of the second harmonic signal, generated by mixing of the two fundamental fields, depends on the temporal overlap of the pulses. As a result, the width of the autocorrelation can be related to the width of the unknown pulses.

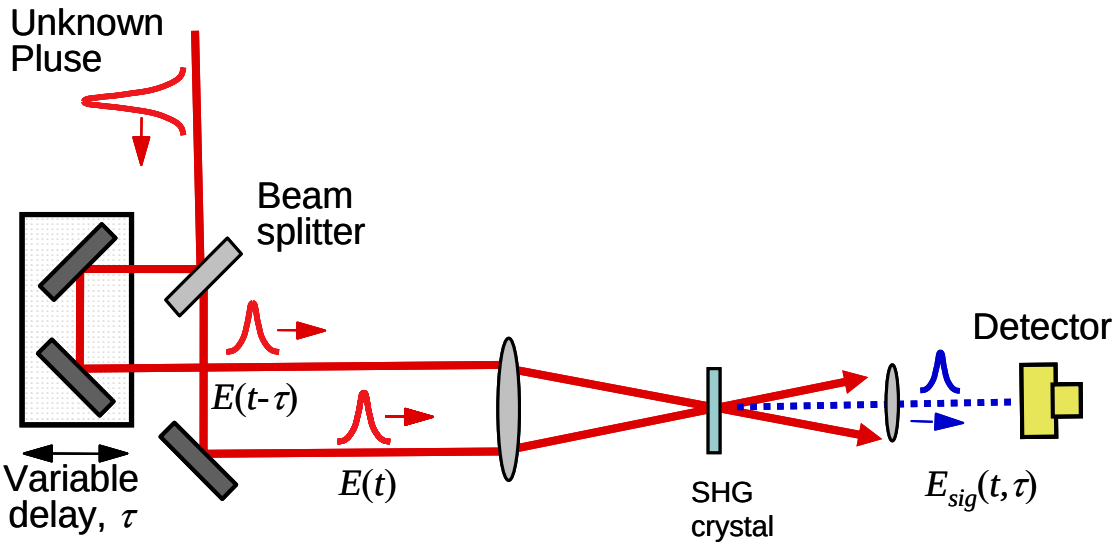

Figure 1 – 1: Experiment layout for an intensity autocorrelator using second-harmonic generation. An unknown pulse is split into two, one is variably delayed with respect to the other, and the pulses are overlapped in an SHG crystal. The SHG pulse energy is measured vs. delay, yielding the autocorrelation trace.

Actually, the pulses width can be related to the autocorrelation width only if we have pulses without much temporal structure. Otherwise, the autocorrelation doesn't uniquely yield the intensity of the pulse and numerous ambiguities can generate the same autocorrelation trace [9]. Worse, we fail to extract the phase information from the autocorrelation because of one-dimension phase retrieval problem and ambiguities [10]. Even though we use a combination of the autocorrelation and spectrum to retrieve the intensity and phase of the pulse, it is not sufficient to yield the unique pulse.

Despite these ambiguities and lack of the phase information of the pulses, the autocorrelation with measuring spectrum has remained the standard measurement technique of ultrashort pulses and the autocorrelators give a rough estimate of the pulse width for many years. This is mainly because there were no better methods. However, a wide range of applications of ultrashort pulses, including Chemistry and Biology,

requires not only the phase information but also the intensity of the pulses with no ambiguities.

1.2 FROG

What is measuring ultrashort pulses? This is a very complicated question because pulses have four dimensions (x, y, z, t) and pulses normally suffer from a couple of distortions such as spatial chirp and pulse-front-tilt, even though the distortions affect little. For almost all cases, however, knowledge of the intensity and phase in the time domain (or the frequency domain) is sufficient to determine the pulse. The expression for the pulse in the time domain:

$$E(t) = \mathrm{Re}\left\{\sqrt{I(t)}\exp\left[i(\omega_0 t - \phi(t))\right]\right\}$$

where I(t), $\phi(t)$, and ω_0 are the intensity and phase of the pulse, and a carrier frequency respectively. Equivalently, The expression for the pulse in the frequency domain:

$$\tilde{E}(\omega) = \sqrt{S(\omega)}\exp\left[-i\varphi(\omega)\right]$$

where $S(\omega)$ and $\varphi(\omega)$ are the spectral intensity and phase of the pulse respectively. Once we get the information of the pulse in one domain, we can transform it to the other domain using Fourier-Transformation. In this paper, measuring ultrashort pulses means measuring the intensity and phase of the pulse in one domain.

The autocorrelation is an ultrashort-pulse measurement technique that operates purely in the time domain and measuring spectrum is another ultrashort-pulse measurement technique that operates purely in the frequency domain. In general, the measurement techniques have the one-dimensional phase-retrieval problem that is not

solved in almost all cases of practical interest, when trying to extract the phase information from the measurement techniques [9]. An ultrashort-pulse measurement technique in the hybrid domain, an intermediate domain such as the time–frequency domain, might have a problem that can be solved in almost all cases of practical interest. Even though it is not quite intuitive, the two-dimensional phase-retrieval problem in the time-frequency domain has an essentially unique solution when we have certain additional information such as that it is zero outside a finite range of values of the time and the frequency [9, 11, 12, 13]. In experiment, we can assume that the additional information is always true. Frequency-Resolved-Optical-Gating (FROG) is the measurement technique with the two-dimensional phase-retrieval problem that can be solved in the time-frequency domain.

Simply, imaging the nonlinear signal in an autocorrelator to the entrance slit of an imaging spectrometer turns an autocorrelation trace into a FROG trace. Unlike the autocorrelation which records the nonlinear signal intensity for each delay, the FROG records spectrum of the nonlinear signal for each delay. As a result, a FROG trace, a spectrally resolved trace, is a two-dimensional image in which the delay is running in one dimension and the wavelength in the other. Spectrally resolving yields the Fourier Transform of the signal field, instead of the signal intensity, with respect to time and a camera only can measure the squared magnitude. Hence, the mathematical expression for FROG traces is:

$$I_{FROG}(\omega,\tau)=\left|\int_{-\infty}^{\infty}E_{sig}(t,\tau)\exp(-i\omega t)dt\right|^2$$

where $E_{sig}(t,\tau)$, which depends on the nonlinearity used, is the signal electric field. For instance, for the polarization gate FROG, one of the third-order FROG, the signal electric field is:

$$E_{sig}(t,\tau) = E(t)\left|E(t-\tau)\right|^2,$$

if we ignore all constants. Because while the autocorrelation uses intensities of pulses, instead of electric fields, the FROG uses intensities after the Fourier transformation with respect to time, the FROG trace expression contains the phase information in the pulse, which is the most important distinction of FROG from the autocorrelation.

In practice, another useful, important feature of FROG is redundancy. The resulting FROG trace is a time-frequency plot with an N x N array of points, which are used to determine N intensity points and N phase points. There are thus many more degrees of freedom in the FROG trace with an N x N array of points than in the pulse with 2N points. As a result, a measured trace that has been contaminated by systemic error or random error can not correspond to an actual pulse. Similarly, even if one dimension does not have enough resolution to resolve fine structure in pulses, it is possible that information in the other dimension retrieves the structure in the pulses due to the redundancy of information in FROG traces.

The conventional FROG algorithm is called general projections, which is so reliable to the others that most pulses can be retrieved with it alone, and is used in the phase- retrieval problem [14, 15, 16]. Figure 1-2 shows the generalized-projections technique. In the figure, while the upper elliptical region represents the signal fields satisfying the mathematical-form constraint, the lower elliptical region represents the

signal fields satisfying the data constraint. The intersection of two elliptical regions, in which the signal fields satisfy, is the solution.

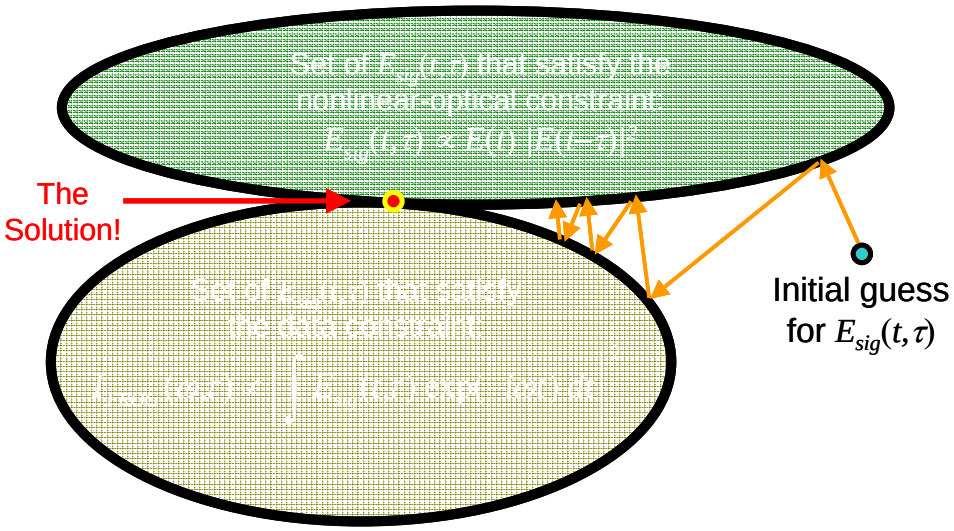

Figure 1 – 2: Generalized projections applied to PG FROG. Moving to the closest point in one constraint set and then the other yields convergence to the solution.

This algorithm starts with an initial guess at an arbitrary point in signal-field space, which satisfies neither constraint. By making projections from the arbitrary point, the solution is found. In the first iteration, the algorithm makes a projection onto one of the constraint sets, which consists of moving to the point in the set closest to the initial guess. From the point, the algorithm projects onto the other set, moving to the point in the set closest to the first iteration. This process is continued until the solution is found. If the two constraint sets are convex, convergence is guaranteed. However, if they are not convex, the projection is not necessarily unique, and convergence cannot be guaranteed by generalized projections. Although the algorithm may stagnate at a constant value, the method is quite robust in FROG.

1.3 FROG BEAM GEOMETRIES

In order to get acquire a FROG trace, we need to get a nonlinear signal, which is spectrally resolved, for each delay. Depending on the nonlinear optical processes, we can make several FROG beam geometries. Figure 1-3 shows various beam geometries for FROG measurements of ultrashort pulses.

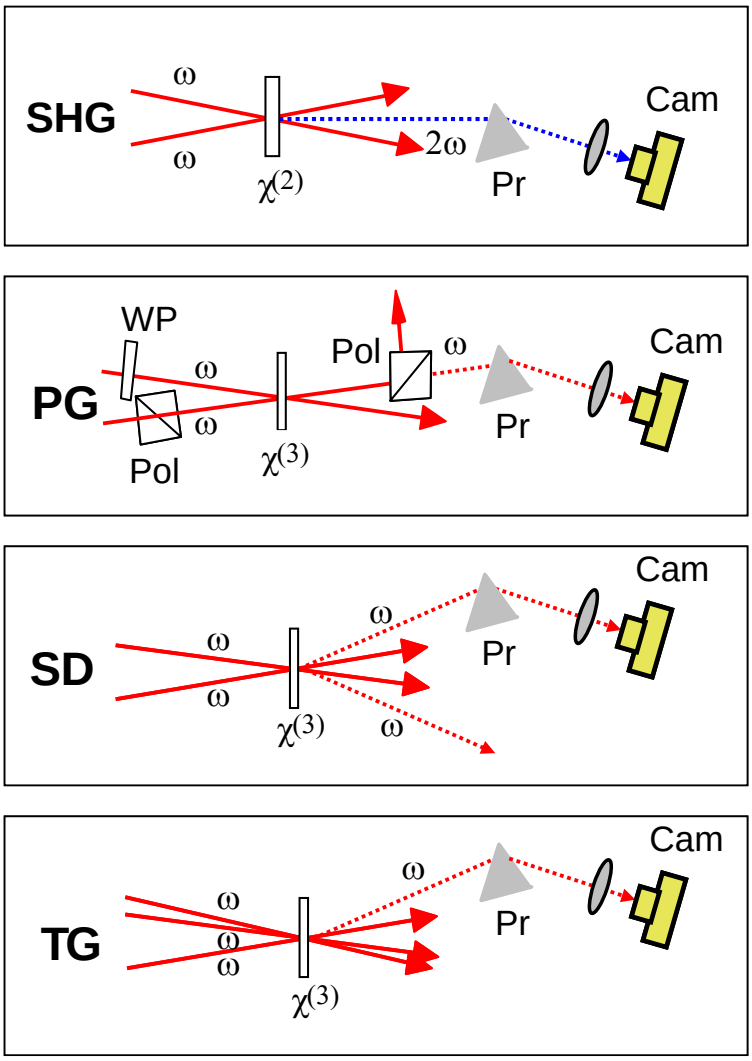

Figure 1 – 3: Various beam geometries for FROG measurements of ultrashort pulses. The combination of Pr (prism) and lens represents a spectrometer. WP, wave plate; Pol, polarizer; SHG, second-harmonic-generation FROG; PG, polarization-gate FROG; SD, self-diffraction FROG; TG, transient-grating FROG.

The most sensitive version in these FROG beam geometries is the second-harmonic-generation FROG, because it uses second-harmonic process, while the other FROG geometries use third-nonlinear process. SHG FROG is commonly used to measure unamplified pulses directly from Ti: sapphire oscillator pulses, and most of pulse measurement devices are based on this process, not only FROG but also spectral phase interferometry for direct electric-field reconstruction (SPIDER) [17]. The disadvantage of SHG FROG is that it generates unintuitive traces that are symmetrical with respect to delay.

PG FROG traces are quite intuitive and PG FROG yields complete and unambiguous pulse intensity and phase of the pulses. Additionally, PG process is automatically phase-matched. However, it requires high-quality polarizers which are very thick and introduce pulse distortion [18].

Unlike PG FROG, SD FROG doesn't require polarizers, and so it is useful for measuring UV pulses. On the other hand, SD is non-phase-matching process which requires that the nonlinear medium must keep thin and the angle between two beams small [18, 19].

TG FROG is the most versatile all-around beam geometry for FROG measurements for amplified ultrashort pulses because TG FROG is the geometry that is both phase-matched and free of large chunks of material, which can cause pulse distortion, such as polarizers. The disadvantage of TG FROG is complexity. It uses a three-beam geometry, requiring that the input beam be split into three pulses and the three beams be overlapped in time and space at nonlinear medium. As a result, TG FROG beam geometry is only occasionally used for pulse measurement [20].

1. 4 MULTI-SHOT AND SINGLE-SHOT FROG

In multi-shot FROG beam geometries, the relative delay is varied by scanning a mirror position. One spectrum can be measured at a time because one value of the delay can be set at a time. By increasing (or decreasing) the relative delay between two pulses, another spectrum can be measured at the delay. In multi-shot geometries, the delay increment corresponds roughly the time resolution even though the time resolution is a function of the crossing angle and the beam geometry. In order to produce a FROG trace, the multi-shot geometries require measuring spectra over many laser pulses. As a result, we need to assume that the intensity and phase of the pulse is the same for each pulse during the measurements. This is usually a pretty good assumption for Ti:Sapphire oscillators. However, there are a lot of laser sources such as supercontinuum and a free electron laser, which vary from shot to shot, and so can not satisfy this assumption.

When we consider measuring these pulses, a single-shot measurement technique is a solution. Depending on what kind of pulses we have, we can make any single-shot FROG geometry for each nonlinear optical process. Essentially, the single-shot FROG geometries are the same with the multi-shot geometries, except that the single-shot geometries use cylindrical optics, instead of spherical optics, and the beams are crossed at a large angle in order to generate enough delay range while the multi-shot geometries use a small crossing angle to avoid the transverse geometrical smearing.

For a single-shot SHG FROG geometry, as an example, the input pulse is split into two beams, and a cylindrical lens focuses the two beams to a line with a large angle. Figure 1-4 shows beam crossing in nonlinear medium for a single-shot FROG geometry.

Note that, in the center, the beams overlap in time (zero delay). However, toward the top of the figure, one pulse precedes the other, while, toward the bottom of the figure, the other precedes the one. The delay varies transversely cross the medium [21].

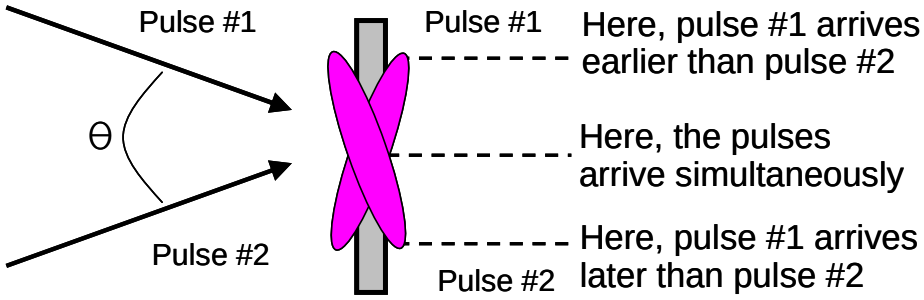

Figure 1 – 4: The relative delay between crossed input beams is zero along the center dashed line. While, in upper part of the nonlinear medium, one beam precedes the other, in lower part, the other precedes the one. This effect allows us to achieve single-shot operation.

If we image the nonlinear medium onto the entrance slit of an imaging spectrometer, a camera can capture a spectrally resolved trace, in which the delay varies vertically and frequency varies horizontally. As a result, the image captured by the camera is a single-shot FROG trace. Because each shot can generate a FROG trace, we don't need to assume that the intensity and phase of the pulse should be identical with the whole set of the pulses during the measurement.

If we have a pulse with certain pulse duration and want to measure the pulse using a single-shot geometry, the maximum delay generated by crossing two beams in the shingle-shot FROG geometry should be greater than the pulse duration. The maximum range of delays, $\Delta\tau$, is given by:

$$\Delta\tau = 2(d/c)\tan(\theta/c) \approx d\theta/c$$

where Θ is the angle between the beams in the nonlinear medium, and d is the beam diameter, and c is the speed of light. (The approximate result can be used for a small angle Θ.) In order to generate more delay range, we need to increase either the beam diameter or the beam crossing angle (or both). Now, the delay is a function of transverse coordinate, x, in a two-dimensional array camera. If we set the delay to be zero at the center of the beams, the delay, τ , is given by:

$$\tau(x) = 2(x/c)\sin(\theta/c) \approx x\theta/c$$

In experiment, it is not easy to find out the delay $\tau(x)$ as a function of x, because, in the nonlinear medium, we have the different speed of light and the different angle due to the index of refraction of the medium. Normally, we use a calibration to find out the function of x of the delay.

One of disadvantages of the single-shot FROG geometries is that they require more energy than the multi-shot geometries do because the single-shot uses a cylindrical focus instead of a spherical focus. Another experimental issue I want to mention is that, in a single-shot geometry, the beam spatial profile need to be smooth. If the beam does not have a smooth profile, we can use either spatial filter or expanding the beam. Both ways cause decreasing the beam energy too. As a result, if the pulse energy is not strong enough, then it is not easy to measure the pulse using single-shot FROG geometries which are very robust and reliable measurement techniques.

1. 5 A SIMPLIFIED FROG: GRENOUILLE

If we have strong enough pulse energy from ultrashort-laser sources, using a single-shot FROG geometry is a better idea because it is simple and inexpensive, comparing with a

multi-shot FROG geometry. However, we still need to make considerable alignment effort to build it. In the other hand, making a lot of alignment effort means that it has more changes to introduce pulse distortions during the measurements. Therefore, this calls for a simplified version of FROG. In 2001, O'Shea et al. demonstrated a very simplified version of FROG, called GRENOUILLE (Grating-Eliminated No-nonsense Observation of Ultrafast Laser-Light E-Field) [8]. The GRENOUILLE, which consists of only four optical elements, is a single-shot FROG device based on SHG process for measuring ultrashort laser pulses. This device is so simple that, once set, it never misaligns.

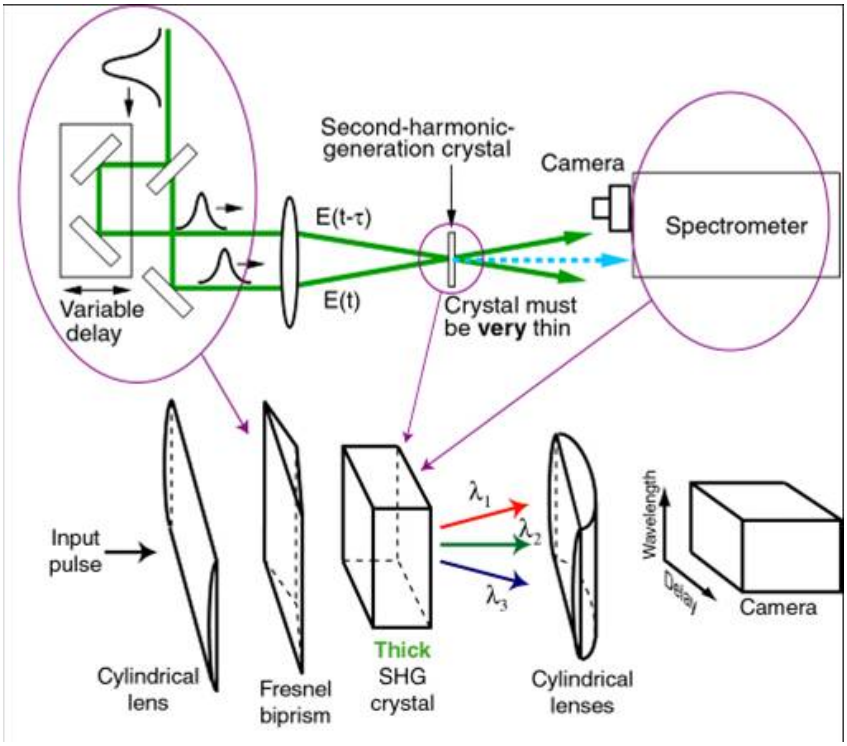

Figure 1 – 5: GRENOUILLE uses a Fresnel biprism to replace the beam splitter, and delay line, and beam-recombination optics. It maps delay to position at the crystal. GRENOUILLE also utilizes a thick SHG crystal acting as both the nonlinear-optical time-gating element and spectrometer.

Figure 1-5 shows an autocorrelator based on SHG process. If a spectrometer replaces the camera in the figure, then the autocorrelator turns into a SHG FROG. Figure 1-5 shows a FROG device and the GRENOUILLE device. In GRENOUILLE, a Fresnel biprism replaces the beam splitter and delay line and a thick crystal replaces the thin crystal and spectrometer in the FROG.

One key innovation in GRENOUILLE is using a Fresnel biprism. When a Fresnel biprism, a prism with an apex angle close to 180 degree, is illuminated with a wide beam, this splits the beam into two beams and crosses them at a large angle. Like conventional single-shot FROG geometries, GRENOUILLE requires crossing two beams at a large angle where the relative beam delay is mapped onto horizontal position at the nonlinear medium. In GRENOUILLE, the beams that are split and crossed by a Fresnel biprism are automatically aligned in space and time. This makes the device a lot easier and simpler.

Another key innovation in GRENOUILLE is removing a spectrometer in the device. Because FROG traces need to be spectrally resolved, in order to do this, use of a spectrometer is necessary. However, the thick crystal in the GRENOUILLE has a relatively small phase-matching bandwidth, so the phase-matched wavelength produced by the crystal varies with angle. Eventually, the thick crystal acts like a low resolution spectrometer. Even though it has a low resolution, this simplifies the FROG device significantly and GRENOUILLE works perfectly for pulses with a wide bandwidth.

GRENOUILLE has a few elements and so is inexpensive and we can make it very compactly. (Actually, a company Swamp Optics sells a commercial GRENOUILLE with 37 x 7 x 5 cm in dimensions and ~2kg in weight.) Also, GRENOUILLE operates single-shot and it is considerably more sensitive than other pulse-measurement devices. In

addition to this, recently, Arturk et al. found that GRENOUILLE could measure pulse distortions such as spatial chirp and pulse-front-tilt of ultrashort pulse and he developed another version of GRENOUILLE, which could measure very short pulses with pulse duration about 10fs, using reflective components instead of transmissive components.

Consequently, it is clear that the invention of FROG is a breakthrough not only in the ultrashort pulse measurement field but also in application fields using the ultrashort pulse because now they can know what pulse they have. Recently, the applications of the ultrashort pulse have been extending over many other fields such as chemistry and biology where they are not professional in optics and lasers. Therefore, it is no doubt that the next significant improvement in the ultrafast-laser-pulse field is the invention of GRENOUILLE, because now they can measure their pulses easily even though they are not good at optics or laser.

CHAPTER 2

CONTINUUM MEASUREMENT GENERATED FROM PHOTONIC NANOWIRE USING MULTI-SHOT SFG X FROG

Portions of the work presented in this chapter originally appeared this chapter originally appeared as a paper by the author:

M. A. Foster, J. M. Dudley, B. Kibler, Q. Cao, **D. Lee**, R. Trebino, and A. L. Gaeta, "Nonlinear pulse propagation and supercontinuum generation in photonic nanowires: experiment and simulation," Appl. Phys. B 81, 363-367 (2005)

2. 1 INTRODUCTION

The generation of supercontinuum (SC) has been demonstrated by injecting high power pulses near the zero dispersion wavelengths of photonic crystal fibers (PCF) [22]. Similar broadband SC has also been observed in standard optical fiber tapered to a strand diameter ~2 μm where the tapering introduces dispersion and nonlinearity characteristics similar to those of PCF [23]. Since these demonstrations, much research was conducted to understand and control the process. This research leads to breakthrough applications in such fields as optical frequency metrology and optical coherence tomography [24, 25, 26]. Two properties of these fibers make them ideally suited to efficient broadband nonlinear frequency generation. The large index contrast of glass (1.45) to air (1.0) and small core diameters of approximately 2 μm provide high modal confinement and a significant waveguide contribution to the dispersion. With appropriate choice of waveguide parameters, high effective nonlinearities are achieved with low group-velocity dispersion (GVD) at the pump wavelength [27, 28, 29]. While researchers have investigated

extensively the control of the nonlinear interaction by altering the GVD of fibers with core diameters larger than the pump wavelength, more recently the regime of sub-wavelength diameter waveguides has attracted interest [30, 31]. Waveguides of sub-wavelength diameters, known as photonic nanowires, can provide maximal effective nonlinearities as well as exotic dispersion profiles [32, 33, 34].

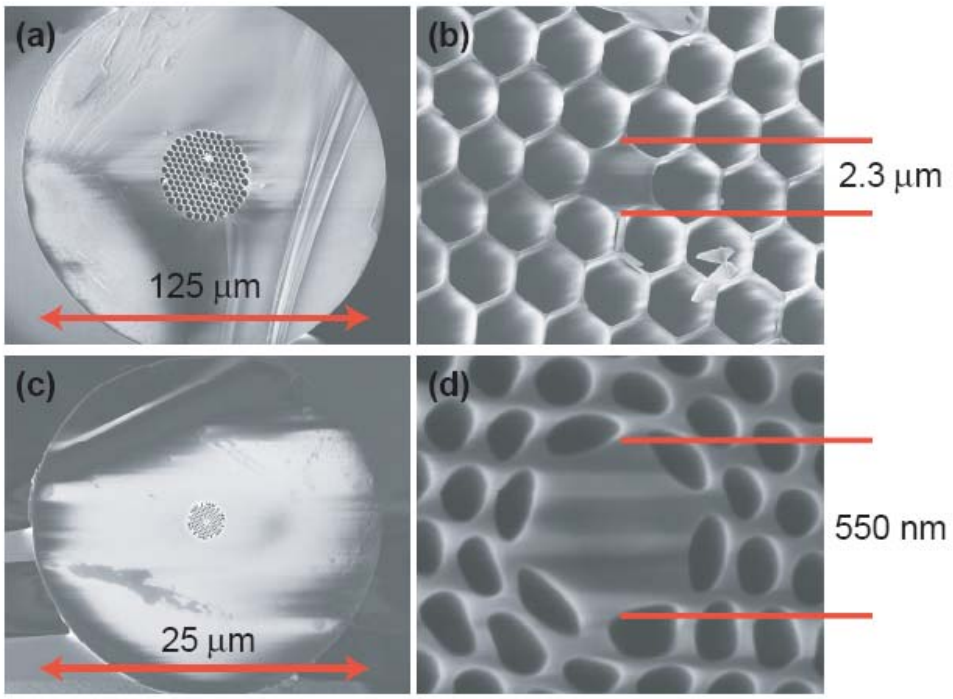

Figure 2 – 1: SEM images of the (a), (b) untapered and (c), (d) tapered fiber cross sections. A scanning electron microscope (SEM) was used to image the cross-section of the fiber and determine the core diameter. The upper left (a) shows the fiber cross sections before tapering and near the center of the taper. Using the SEM, the core diameter was measured at several places along the taper. While the air structure changes in size and shape, the ratio of the core diameter to the outer diameter of the fiber was found to be a constant 0.02 as seen in Fig. 2 - 2. Therefore, measurement of the outer diameter of the taper with an optical microscope provides an accurate estimate of the core diameter without breaking the fiber.

Fabrication of low-loss nanowires was demonstrated using the flame brush technique [35]. In order to fabricate a waveguide structure with sub-wavelength core diameter, we tapered a high airfilling fraction 2.3-μm-core microstructure fiber from BlazePhotonics. It is important to keep the air-glass structure from collapsing by closing off the ends of the fiber and using a sufficiently high pulling speed [36]. These processes allowed for tapering the core down to a 400-nm diameter, maintaining the air cladding structure.

(a) and (b) in Figure 2 – 1 show the scanning electron microscope (SEM) images of a high airfilling microstructure fiber with 2.3-μm-core size. After making a taped microstructure fiber, the cross sections ((c) and (d)) show that the 550nm core is still surrounded by air claddings without collapsing. Because of this, we can use the model, in which a glass core is surrounded by an air cladding, for calculating GVD properties. Figure 2 – 2 shows the results that the core diameter is measured at several places along the taper using the SEM. While the air structure changes in size and shape, the ratio of the core diameter to the outer diameter of the fiber was found to be a constant 0.02

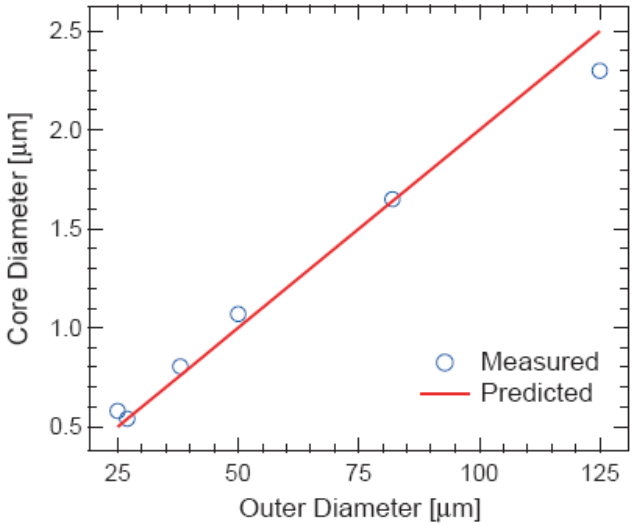

Fig. 2 – 2: The core diameter and outer diameter measured at various points along the fiber taper

Specifically, durable sub-wavelength waveguides were fabricated by tapering standard microstructure fibers such that the core diameter becomes sub-wavelength in scale. The outer diameter of these fibers is tens of microns making them robust to manipulation as well as to changes in their environment. Using these fibers, ultra-efficient octave spanning SC generation was demonstrated using both nanosecond and femtosecond pump pulses [35, 37]. This continuum is characterized by a blue-shifted spectrum generated well into the visible with little spectral power in the infrared. Understanding of the dynamics leading to these characteristic spectra will allow for greater control and applicability of supercontinua generated from nanowires.

2. 2 WAVEGUIDING PROPERTIES

The properties of the high air-filling-fraction microstructure fibers used for SC generation are adequately modeled as a glass core surrounded by an air cladding [38]. With this

model, we analyzed the confinement of the fundamental mode as the size of the core is reduced [34]. As seen in Figure 2 - 3, for cores larger than the wavelength of propagating light, the mode field diameter (MFD) follows the core diameter. However, as the core becomes smaller than the wavelength of light, the MFD reaches a minimum and then diverges rapidly. This behavior leads to a specific waveguide diameter which maximizes the effective nonlinearity (see Figure 2 - 3) and we find that the maximally nonlinear waveguide is sub-wavelength in size. For example, for 800-nm light produced by a Ti:sapphire laser, a fiber core diameter of 550 nm optimizes the nonlinearity.

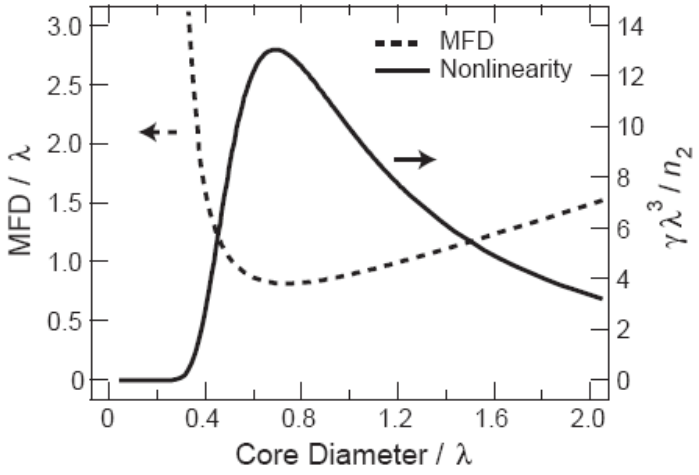

Fig. 2 – 3: The mode field diameter (MFD) and the normalized effective nonlinearity $\gamma\lambda^3/n_2$ for a circular glass (index of 1.45) waveguide in air (index of 1.0).

The sensitive dependence of the MFD to the core diameter yields a substantial waveguide contribution to the group-velocity dispersion (GVD). Using the glass-rod-in-air model, the GVD of several sub-wavelength waveguides was calculated, and the results are shown in Figure 2 – 4. For the 2.3-μm-core waveguides commonly used for SC generation, the first zero-GVD point is shifted into the visible while the second zero-

GVD point lies in the infrared. For nanowires, the larger waveguide contribution to the GVD pushes both zeros into the visible [33, 34]. With appropriate choice of the core size, the second zero-GVD point can be positioned near the pump wavelength to yield anomalous, normal, or zero GVD.

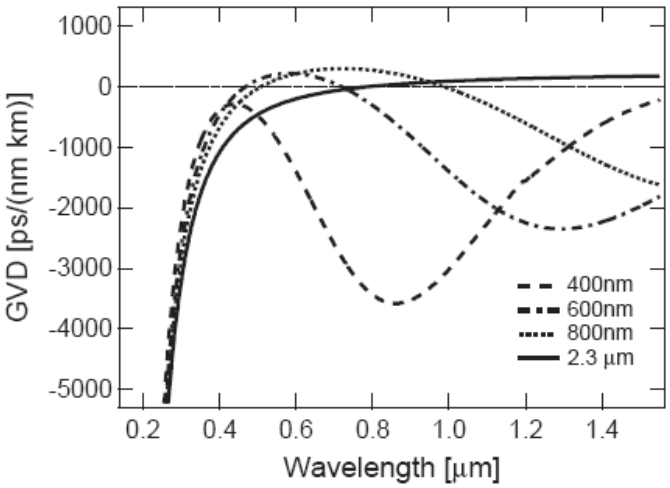

Fig. 2 – 4: Group-velocity dispersion (GVD) of a glass rod in air for core diameters of 400 nm, 600 nm, 800 nm, and 2.3 μm.

For sub-wavelength waveguides a significant fraction of the modal power resides in the evanescent field. This portion of the mode is interacting directly with the air-glass interfaces. Any imperfections in this structure, such as surface roughness, will lead to scattering and loss [39, 40]. For longer wavelengths, a larger fraction of the power lies in the evanescent field, therefore one would expect a larger loss. For example, Figure 2 – 5 shows the calculated fractional power in the core as compared to the measured transmission of a tapered microstructure fiber with a 400-nm minimum core diameter. In this case, the relative loss becomes significant for wavelengths with more than a 25 percent of the power in the evanescent field.

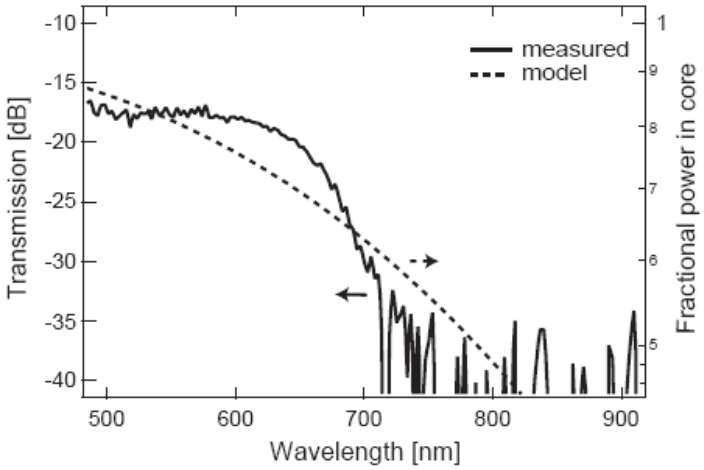

Fig. 2 – 5: Measured transmission and calculated fractional power in the core for a 400 nm waist diameter tapered microstructure fiber.

2. 3 EXPERIMENTS

The method by which we fabricate sub-wavelength waveguides was described previously [35]. The technique consists of tapering a 2.3-μm core microstructure fiber using a standard flame-brush technique [41] such that the microstructure cladding remains intact. By this method, the core is reduced to a sub-wavelength size over a few centimeters. The taper profiles used in this investigation are shown in Figure 2 – 5. Fibers A and B have similar profiles but different minimum waist diameters of 400 nm and 500 nm, respectively. Fiber C is shorter in length and has a larger minimum waist diameter of 775 nm. Furthermore, Fibers A and B have a centrally located taper with a total fiber length of 20 cm. Fiber C has 56 mm of untapered fiber to the left of the taper and 83 mm to the right.

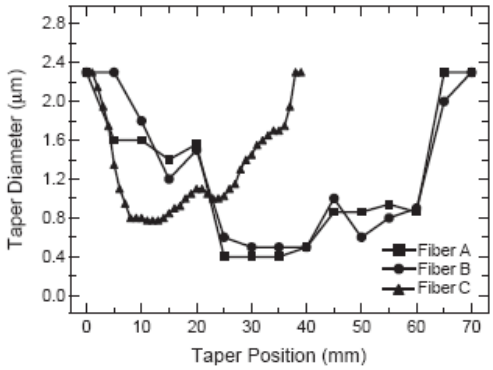

Figure 2 – 6: Core diameter profiles of the tapered microstructure fibers used in this investigation.

Supercontinuum was generated in these fibers using femtosecond pulses from a mode-locked Ti:Sapphire laser. For fibers A and B, the input pulse was 25 fs in duration with 150 pJ pulse energy inside the fiber. For fiber C, the input pulse was 35 fs in duration with 154 pJ pulse energy inside the fiber. The coupling efficiency into the fibers was 60 percent. The generated spectra are shown in Figure 2 – 7. The continuum generated in fibers A and B is substantially blue-shifted from the pump wavelength, whereas the continuum from Fiber C is not. This will be shown to be a result of the significant wavelength dependent loss for fibers with small minimum core diameters. The tapered microstructure fibers produce octave-spanning supercontinuum with 250 pJ pulses. Normally, for the untapered 2.3-μm-core fiber, it requires energies as large as 2 nJ in order to generate an octave of bandwidth. This is because the nanowires maximized the nonlinearity in the tapered region.

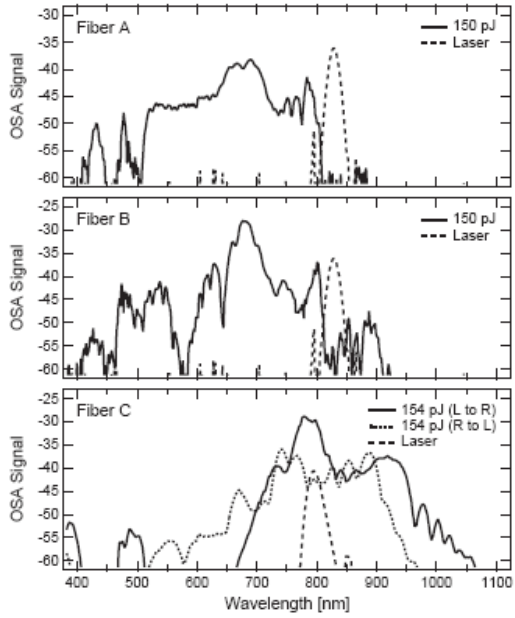

Figure 2 – 7: Generation spectra and input spectra for the three tapered microstructure fibers described, (A), (B), and (C) in Figure 2 – 6.

Continuum was generated by traveling both left to right and right to left through fiber C with different energies (Figure 2 – 8). Unique spectra are generated for each direction of propagation because the transition region affects the generation of the continuum in the taperd fibers. When the pulses propagated from left to right using the rapid transition side, the spectra are shifted to the red side. However, when the pulses propagated from right to left using the gradual transition side, the spectra show symmetries. Additionally, the spectral show a little broadening using 103pJ, 154pJ, and 206pJ of input energies, compared with the other tapered fiber (A and B) because the core size of the taped fiber is bigger than the others, failing to maximize the nonlinearity in the tapered region.

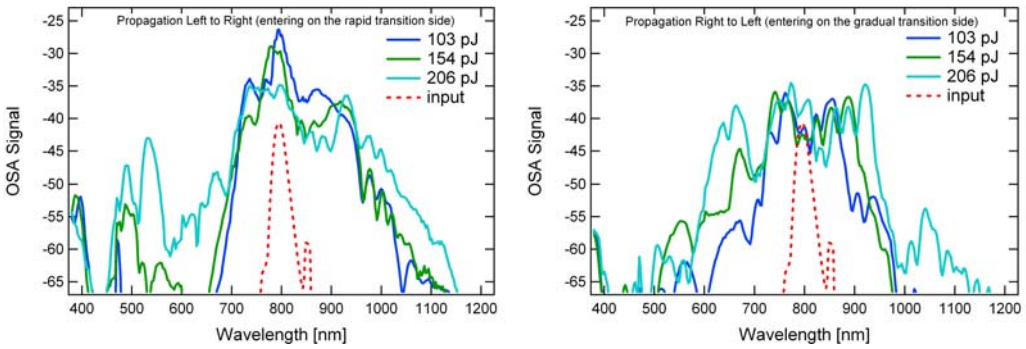

Figure 2 – 8: Generation spectra and input spectra for the tapered microstructure fiber C. The spectra show dependences on propagation directions of the input pulse and input energies.

We measured a spectrogram of the supercontinuum generated in Fiber C for further analysis, using cross-correlation frequency resolved optical gating (X FROG) [41]. This measurement yields a spectrogram representation of the generated supercontinuum pulse (Figure 2 – 9). This measurement was made on supercontinuum generated using 63 fs pulses with a 800 nm central wavelength and 190 pJ pulse energy from a Ti:Sapphire oscillator. The spectrogram representation gives insight into the temporal properties of the generated spectral components. Spectral components in tapered microstructure fibers are generated in two stages. Spectral broadening initially occurs in the microstructure fiber before the taper. Solitons are formed which are then dispersed temporally. When this supercontinuum pulse enters the tapered region, the solitons are exposed to a new dispersive regime which causes some to break up and spectrally broaden in the same way as the initial input pulse in the untapered fiber. This multiple staged SC genration process leads to the branching of the spectrogram seen near zero delay in Figure 2 – 9.

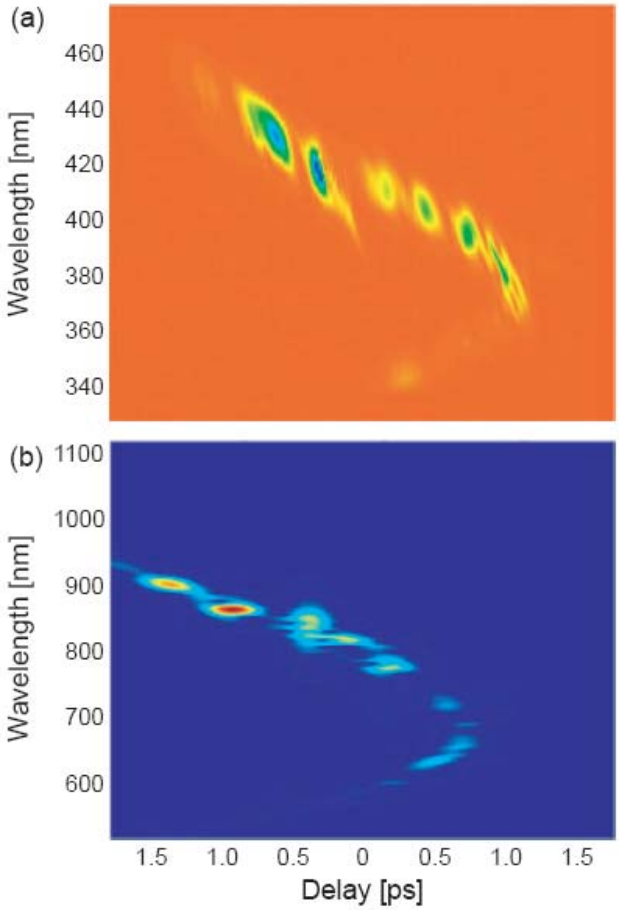

Figure 2 – 9: Spectrogram representation of supercontinuum generated in fiber C (a) measured using cross-correlation frequency resolved optical gating (X FROG) and (b) simulated using the nonlinear envelope equation.

We did FROG measurements of supercontinuum generated in tapered microstructure fiber with 740nm core diameter, angle-dithering X FROG. Figure 2 – 10 shows the schematic diagram of the multi-shot angle-dithering X FROG. The continuum was generated by using very low threshold input energy. The input pulse was generated by a KM Labs Ti:Sapphire Laser, which emitted a 100 MHz train of 40 fs pulses centered at 808 nm. The input pulse energy was about 375pJ before the objective used to launch

the pulse into the fiber. Because different glasses in high-NA microscope objectives cause dispersion, the pulses should be pre-chirped to compensate for dispersion. To do this, we build a pulse compressor between the Ti-Sapphire oscillator and BS1 (not shown in Figure 2 – 10). The pulse compressor is adjusted in order to maximize the bandwidth of the continuum with a given input energy. On the other hand, for a reference pulse, the X FROG algorithm prefers a Fourier-transform-limited pulse and so we build another pulse compressor between BS1 and BS2 (not shown in Figure 2 – 10). With two pulse compressors, we can control the linear chirp of the input pulses to the taper microstructure fiber and the reference pulse.

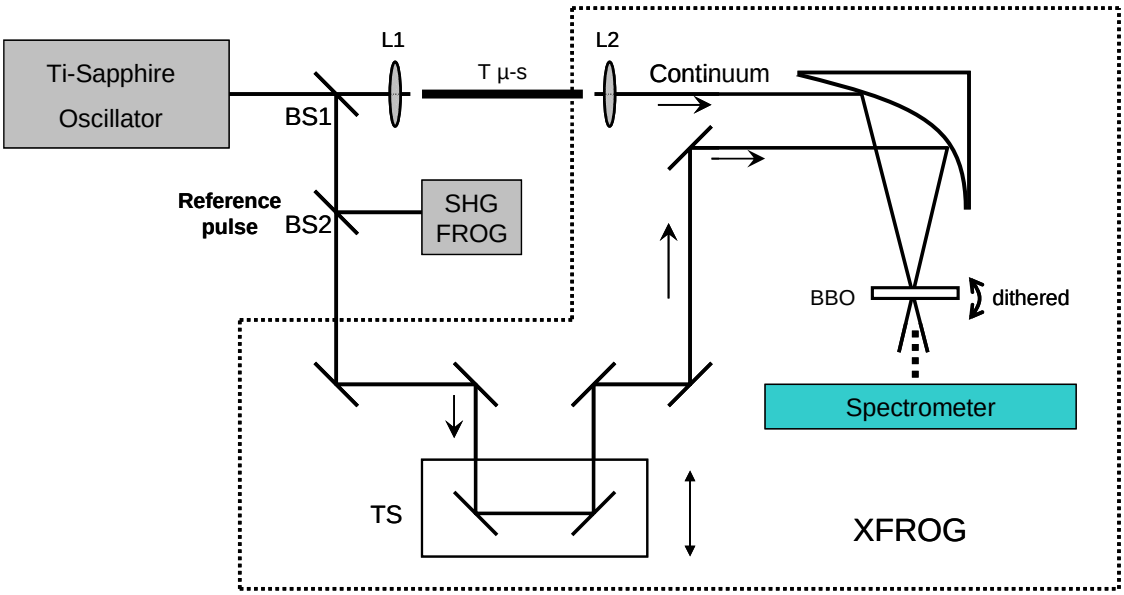

Figure 2 – 10: Schematic diagram of the multi-shot X FROG measurement apparatus: BSs, beam splitters; Tμ-s, taper microstructured fiber; TS, translation stage; L1, objective lens; L2 collimate optics.

The coupling efficiency of the objective lens (L1) is about 60%. So the actual input energy into the fiber is about 225pJ. The tapered part is about 35mm long. The tapered core size was measured as the average of this part. Total tapered and untapered

fiber used in the continuum generation is about 217mm in length. After generating continuum from taper microstructure fiber, for collimating the continuum, we use reflective microscope objective that avoids introducing any chirp by materials and chromatic aberration. The reference pulse is measured by a commercial GRENOILLE (Model 820) which is a SHG FROG and, by adjusting the translation stage, is overlapped temporally with the continuum pulse. In addition to this, in order to make the reference pulse and the continuum overlapped in space, an off-axis replicated parabolic mirror is used to avoid pulse distortions by the transmissive components.

The fiber output was gated by the pump pulse itself in a 1-mm-thick BBO crystal, which achieved phase-matching at all wavelengths by angle-dithering with the amplitude of about 25°. The delay between the measured continuum and the gate pulse was scanned in 1.67-fs steps. The sum-frequency signal pulse generated by the continuum and gate beams was spectrally resolved at each delay in a spectrometer. This yielded an X FROG trace of size 900 x 2048, which was then interpolated into a 1024 x 1024 trace for retrieval of the intensity and phase. The sum frequency generation (SFG) X FROG algorithm retrieved the measured trace. The retrieved results are shown in Figure 2 – 11. In Figure 2 – 11, there are solitons that can be clearly seen in the traces. Also there is a turning point in the trace, whose wavelength should be corresponding to the turning point of the GVD curve of the whole fiber. In Figure 2 – 12, solitons, which are now separated temporal peaks, can also be observed in the temporal plot. In the retrieved spectrum plot, the output continuum, with fine structure, covers almost 500 to 900nm. It is worth to mention that, with this ultra-low input energy, the fiber could overcome a major

limitation resulting from damage to the fiber end faces due to continuous exposure at high optical powers [5].

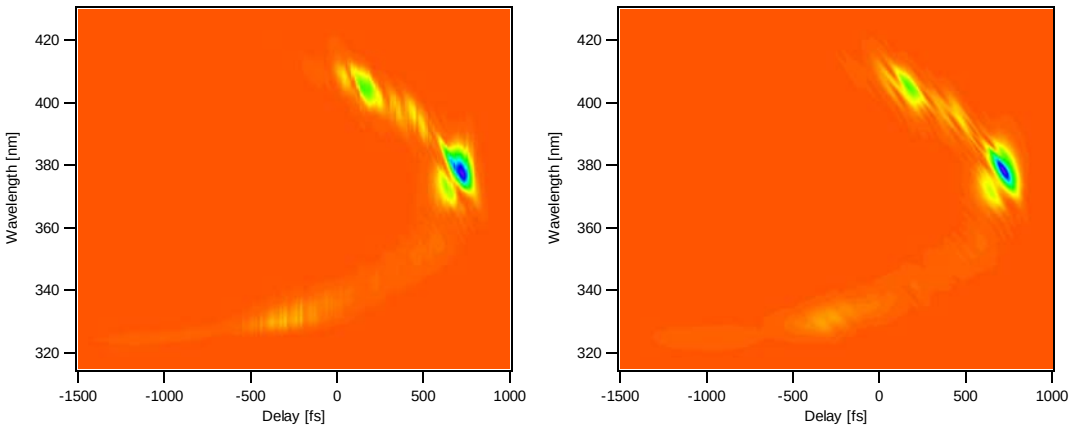

Figure 2 – 11: Measured and retrieved XFROG trace of the continuum from the tapered fiber.

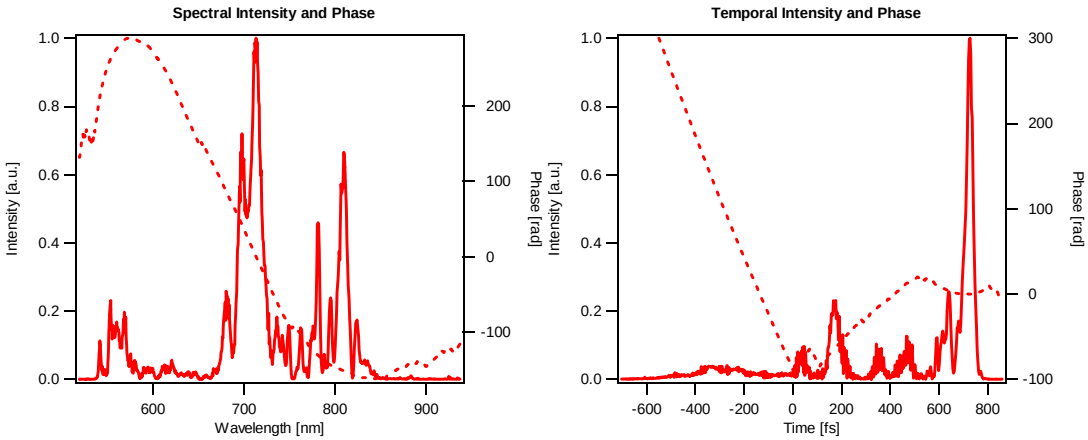

Figure 2 – 12: Retrieved temporal and spectral intensity and phase of the tapered fiber continuum.

2. 4 Conclusions

We have generated and measured continuum from a tapered microstructure fiber using ultra-low input energy and we have shown that the blue-shifting of supercontinuum generated from nanowires is a function of the minimum core diameter of the waveguide. The loss is found to be the primary cause for the observed blue-shifted supercontinuum in the case of a sub-wavelength taper. The results demonstrate that smaller effective interactive area will optimize the effective nonlinearities in such sub-wavelength waveguide. A detailed understanding of the pulse propagation dynamics of nanowires is necessary to facilitate their implementation into photonic devices. In particular, the understanding gained in this investigation will allow for designing nanowires which generate tailored spectral or temporal features.

In angle-dithering X FROG measurement, we observe several important things. First one is that, in the X FROG traces, we always can observe the solitons. Although we can one distinguished soliton in Figure 2-11, in the measured traces of other measurements, several solitons were found.

Secondly, the retrieved traces and retrieved spectrum didn't have fine structure, unlike observation in other long microstructure fibers. The total length of the tapered microstructure fiber is 217mm, including untapered part, even though the tapered part of the fiber is only 35mm. In Figure 2-12, some fine structure starts to be seen in the retrieved temporal intensity. However, it was hard to decide if this structure came from the pulse itself or it came from shot-to-shot pulse energy jitter of the continuum.

Last thing I want to mention about this measurement is that the temporal intensity has several dominant peaks, and the pulse duration of the continuum is not a long pulse.

Normally, the pulse duration of the continuum from microstructure fibers is very long. For example, the pulse duration of the supercontinuum from a 120-mm microstructure fiber was about 3ps when the fiber was pumped by an ultrashort pulse with ~1nJ of energy and ~30fs of duration. However, the Full-width-half-maximum (FWHM) pulse length of this continuum is ~ 40fs if we ignore small humps, in the left side of the retrieved temporal intensity in Figure 2-12, with normalized intensities less than 0.5. This pulse duration is very short, comparing not only with the pulse duration of supercontinuum from microstructure fibers but also with the input pulse used to generate this supercontinuum. This is because, by somehow controlling continuum generation process, the fiber has an ability to compress the input pulse.

CHAPTER 3

A SINGLE SHOT MEASUREMENT OF CONTINUUM FROM BULK FUSED SILICA

3. 1 Introduction

When powerful ultrashort pulses undergo extreme nonlinear spectral broadening, one of the most spectacular phenomena can occur in a wide variety of transparent media and in the photonic crystal fiber. This phenomenon is known as supercontinuum (SC) generation. Since the first observation of the white-light continuum from glass samples by Alfano and Shapiro in the late 1960's [42], SC generation has been the subject of numerous investigations in a wide variety of nonlinear media including solids, liquids and gases. From the start, self-phase-modulation and self-focusing were keys to understand the SC generation mechanism in bulk media and it was clear that self-focusing was an essential ingredient to SC generation, as it was observed that the SC threshold coincided with the critical power for catastrophic collapse. In 1998, SC generation in numerous solid materials has been studied extensively by Brodeur and Chin in which they confirmed that the SC generation was triggered by self-focusing. [22]

One of the breakthroughs for generating white-light was the advent of a new class of optical fiber, known as the photonic crystal fiber (PCF), in the late 1990's. PCF is a new class of optical fiber based on the properties of photonic crystal. Because of its special ability to confines light, which is not possible in conventional optical fiber, the PCF has a lot of applications, such as fiber-optic communications, fiber lasers, nonlinear devices, and high-power transmission. One of the properties of the PCFs is that the group

velocity dispersion (GVD) of fibers, in which the core is made of fused silica, can be zero or anomalous (positive) at 800nm by changing the core size and inner cladding hole-size, while GVD of fused silica is zero at 1.28μm and negative at 800nm. [22] By injecting high power pulses near the zero dispersion wavelength of PCF, the generation of SC has been demonstrated and studied by several groups. [22, 43] Pulse energy of only several nano Joules, relatively small energy compared with the energy for SC generation in bulk materials, is used to generate spectrum extending throughout the entire visible and near-IR regions. The SC generation in PCF is not a highly complex process compared to the generation in bulk materials because SC generation in bulk materials involves an intricate coupling between spatial and temporal effects. [44]

The SC is useful for numerous applications such as optical parametric amplification, excitation spectroscopy, and optical pulse compression. [45, 46] Also, for spectroscopic applications, SC generation is a useful source of tunable ultrafast pulses from the ultraviolet to the infrared. [45] Because of its widespread use, it is necessary to understand the mechanism of the SC generation to control the process. Although these SC mechanisms have been the subject of many research groups over many years, the mechanism of SC generation remains far from being well understood because of its inherent complexities.

Here we demonstrate a single shot transient-grating cross-correlation frequency-resolved-optical-gating (TG X FROG) arrangement using ZnS as a third-order nonlinear crystal and report a single shot measurement of continuum generated from bulk fused silica of 12.5mm, suggesting a method to understand the mechanism of SC generation. A method, which could be used to measure SC, was suggested by X. Gu et al. in 2002. In

his work, he measured SC from the microstructure fiber using a multi-shot cross-correlation FROG (X FROG) and reported that the SC was not smooth and stable. The SC was generated from 152cm of 2-μm- diameter microstructure fiber and the spectral range of the SC was from 400nm to 1600nm. The spectral range about 1200nm could not be phase-matched with a thin BBO crystal even though a sum frequency generation (SFG) X FROG, instead of second harmonic generation (SHG) FROG, was used. [47] In order to solve the ultra-broadband phase-matching condition problem, he used the angle-dithering of a 1-mm BBO crystal. The angel-dithering SFG X FROG, using a relatively thick crystal, which increased the sensitivity of the X FROG, was quite successful because this X FROG device could cover the extremely broad of the spectrum of the supercontinuum from the microstructure fiber, and the retrieved trace and spectrum in the measurements revealed the fine structure of SC and this was confirmed by measuring single-shot measurements of independent spectrum of the SC.

One big issue in measuring continuum is that continuum varies from shot to shot due to the complex mechanism of the generation. When we perform a multi-shot geometry to measure continuum, it is hard to meet the multi-shot measurement assumption, which is all the continuum pulses in the train should be identical. As a result, it calls for a single shot FROG geometry. However, when using sum frequency generation cross-correlation FROG (SFG X FROG), the most sensitive version of FROG, the bandwidth of the continuum generated from bulk fused silica (or a microstructure fiber) is too large to phase-match the continuum with one thin SHG crystal. In order to achieve broadband phase-matching with a single-shot FROG geometry, transient grating

beam geometry, which can phase-match the whole continuum bandwidth simultaneously and is one of the third-order nonlinear-optical beam geometries, is required.

3. 2 Broadband phase-matching Transient grating (TG) X FROG

Phase-matching bandwidth is an issue in developing pulse measurement techniques. With SHG-based measurement techniques, the maximum phase-matching bandwidth with 10-μm-thick BBO crystal, an extremely thin crystal, centered at the wavelength of 700nm, is about 150nm. When the center wavelength goes to 500nm, the 10-μm-thick BBO crystal can phase-match only several tens nm because the crystal dispersion increases significantly near 250nm, the second harmonic of 500nm. [47] Normally, phase-matching the short wavelengths is more problematic than phase-matching the long wavelengths. Around 1100nm, this crystal can phase-match several hundred nm, while it can phase-match only ten nm near 400nm. [Fig. 3 – 1]

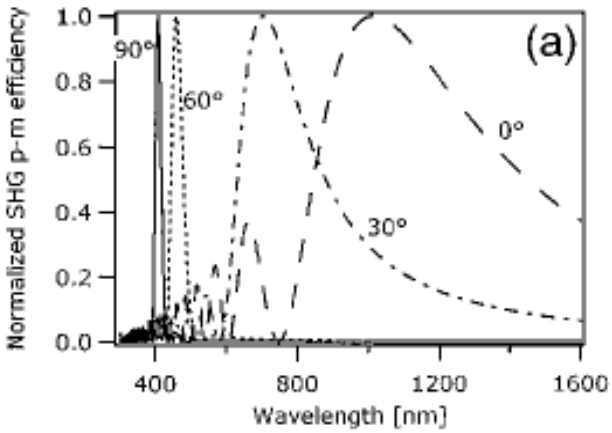

Figure 3 – 1: Normalized SHG phase-matching efficiency of 10-μm-thick BBO for angle ranging from 0° to 90.

In order to achieve broadband phase-matching condition, one of options is using a third-order nonlinear FROG beam geometry such as self-diffraction (SD), polarization gating (PG), or transient grating (TG). [48] However, because SD FROG process is inherently non-phase-matched, the nonlinear crystal need to be extremely thin (this decreases the sensitivity of the FROG device), and this FROG geometry is not possible to measure a broadband pulse like continuum. For PG FROG geometry, it requires highly efficient polarizers, which are not available in UV. Worse, the extinction efficiency of polarizers varies as the wavelength does and, so it is not suitable for broadband continuum even though this process can phase-match the whole wavelength of continuum automatically. One last option is transient grating FROG geometry.

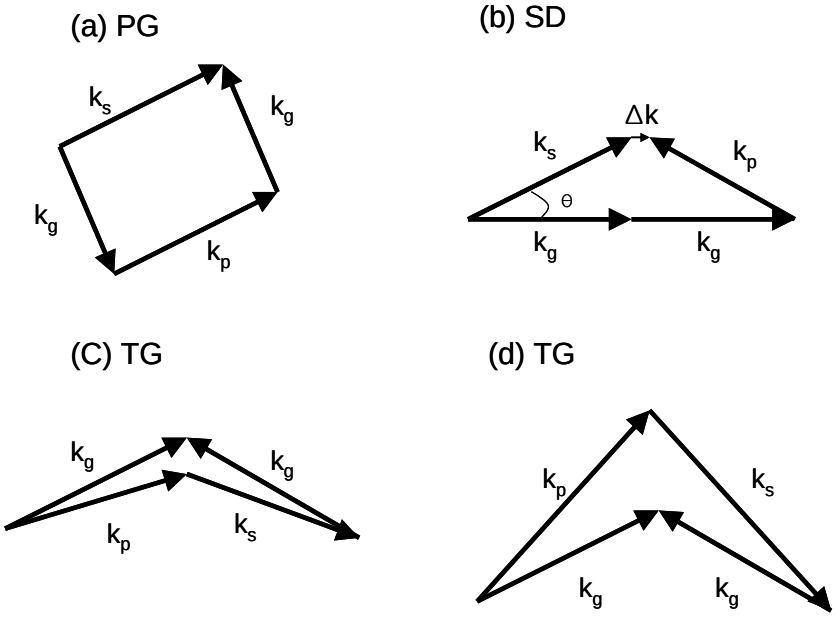

Figure 3 – 2: k-vector diagrams for the three third-order FROG geometries. (a) polarization-gate; (b) self-diffraction; (c) transient-grating (perspective intended to show the parallelogram as in PG is bent out-of-plane); (d) transient-grating with different gate and probe wavelengths like in TG X FROG. In the figure, k_g is a gating vector, k_p is a probe vector, and k_s is a signal vector. Δk is phase-mismatch.

Fortunately, TG FROG fulfills all requirements because transient grating (TG) process can phase match the whole bandwidth of the continuum simultaneously and we can avoid to use any materials that are dependent on wavelengths and introduce pulse distortions in this geometry. Figure 3 – 2 shows k-vector diagrams for the three third-order FROG geometries. It is clear that PG FROG process and TG FROG process are automatically phase-matched when the gate and the probe have the same wavelengths. Even though they have different wavelengths, like the gate centered at 800nm and the probe centered at 600nm, these process can be automatically phase-matched. Note that because TG FROG uses a three-beam geometry, these k-vectors are not in a plane.

Without a shorter event, FROG geometries allow us to measure ultrashort pulses. If we have a shorter reference pulse that has been measured already, it is preferable to use the reference pulse to measure the unknown. If the unknown pulse seems to be complex, using cross-correlation X FROG, which is gating unknown pulse with a known pulse, is more preferable because FROG traces generated by cross-correlation with a known, simple pulse is simpler than FROG traces generated by self-correlation of two (or three) complex pulses. (Normally, in experiment, we use a Fourier-transform-limited pulse as a reference pulse). As a result, when measuring a very complex pulse, gating it with a reference pulse, a Fourier-transform-limited pulse, generates X FROG traces which can be retrieved much easier and faster. Note that even though the reference pulse is longer than an unknown pulse, the X FROG algorithm can retrieve the X FROG traces. In addition to this, this is helpful when the unknown pulse is weak enough that it doesn't yield sufficient signal strength. Continuum pulse from a microstructure fiber is weak

because pulse energy about one nano Joule to generate continuum is used in order to avoid microstructure fiber damage by high peak power. In fact, comparing with pulse energy from an amplified system, also, the energy of continuum pulse from bulk materials is relatively weak because power less than damage threshold should be used. When we try to use a TG FROG geometry, a third-order nonlinear FROG geometry which requires high pulse energy to generate a signal for generating the index grating in the nonlinear medium, pulse energy itself of the continuum is not intense enough to generate TG FROG signal. Therefore, it is necessary to use cross-correlation FROG geometry to achieve a single-shot, broadband FROG. We call it TG X FROG (transient grating cross-correlation FROG). Our TG X FROG arrangement is shown in Figure 3 – 3.

The first beam splitter splits the input beam into two beams. One is for two replicated pump beams. The other is for generating continuum. By the second beam splitter, the one beam is split into two replicas in order to generate two pump beams. These two pump beams are overlapped in time and space and then form an index grating (transient grating) in the nonlinear medium. The other beam goes into fused silica to generate continuum and the beam energy is controlled by the combination of a wave plate and a polarizer. The continuum generated from fused silica is crossed and overlapped in the nonlinear medium and diffracted by the transient grating generated by the two pump beams to produce the signal. The four beam angles (three input beams and one signal beam) in TG geometries take the form of the BOXCARS arrangement. [49] In other words, the signal appears as spots in the corners of a rectangle on a card placed in the beam. Now, the signal is sent to an image spectrometer and a camera can capture the

spectrally resolved TG X FROG trace gated by the known pump pulse which is characterized by a SHG FROG.

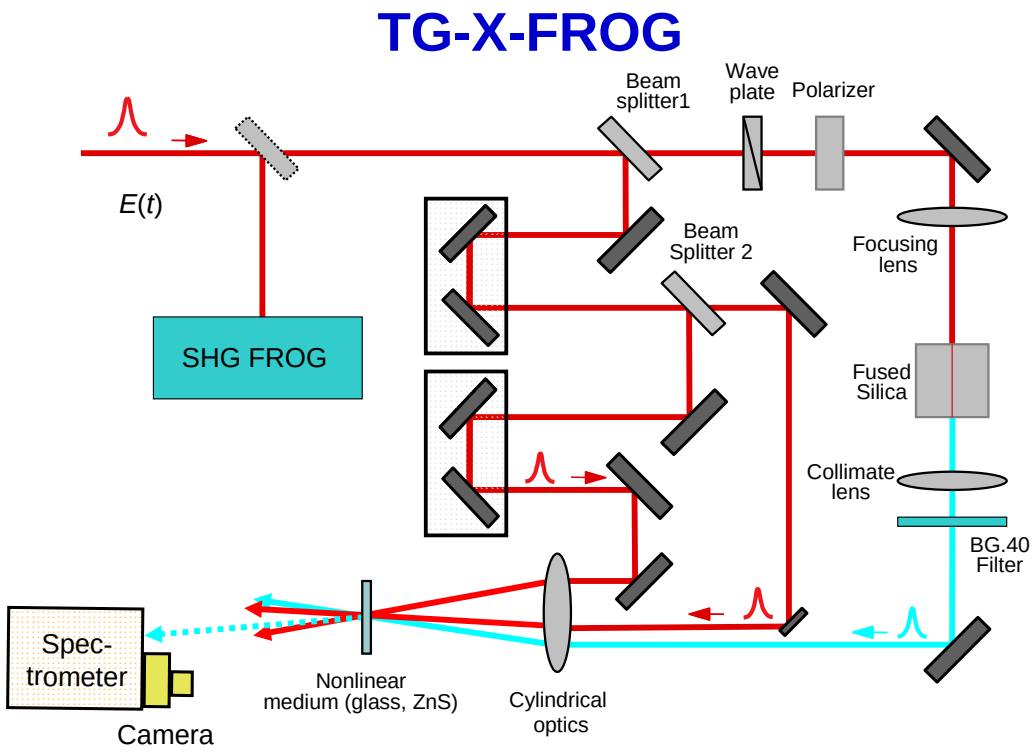

Figure 3 – 3: Schematic diagram of the TG X FROG measurement arrangement. The input beam is measured by a SHG FROG and split into three beams. Two are pump beams. The other beam generates continuum from fused silica. The continuum id filtered by a BG. 40 filter. The three beams are overlapped in time and space in the nonlinear medium. We use cylindrical mirrors in our experiment, instead of cylindrical lenses, for making them crossed and overlapped in nonlinear medium in order to minimize the continuum distortions. We use a lens in the figure because it is easy to understand the arrangement conceptually.

3. 3 Experiments

The input pulse is 800-nm pulses from a Ti:Sapphire regen amplifier and is ~200-fs long, ~340 μJ in energy, and at a 1-kHz-rep-rate. This pulse is measured by a commercial GRENUOILLE (Model 850), which is a SHG-based FROG, in order to use it as a reference pulse.

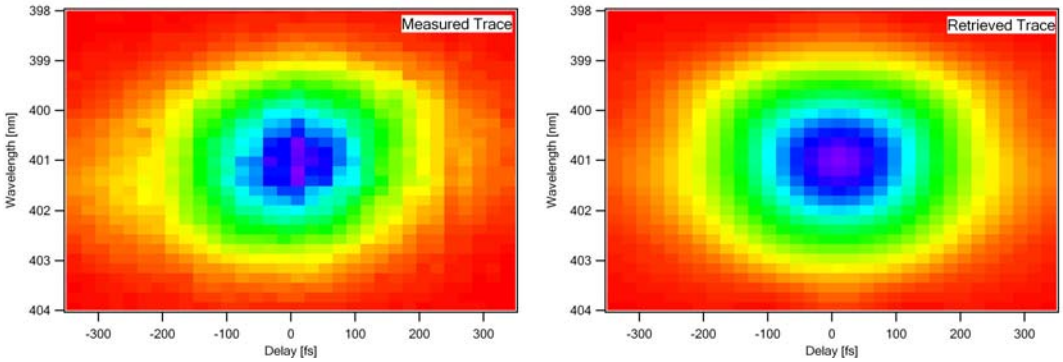

Figure 3 – 4: Measured (left) and retrieved (right) traces for the reference pulse measurement centered at 802nm.

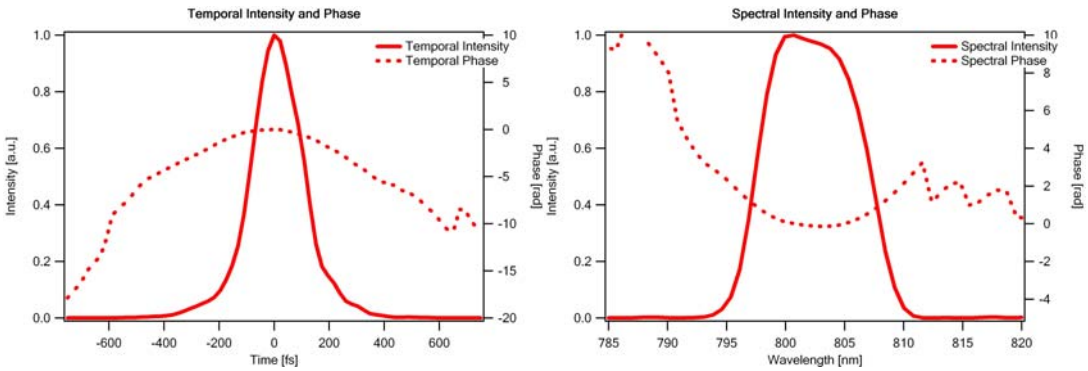

Figure 3 – 5: Left: The retrieved spectral intensity and phase of the reference pulse. Right: The temporal intensity and phase measured using GRENOUILLE.

Figure 3 – 4 shows the measured and retrieved traces for the reference pulse and the agreement is good. The FROG error for the 128X 128 traces is about 0.85%. Figure 3 – 5 shows the retrieved intensity and phase of the reference pulse using a commercial

GRENOUILLE from the Swamp Optics (Model 8-50). The reference pulse's measured FWHM duration and bandwidth that GRENOUILLE retrieved are 209fs and 9.9nm respectively. In order to compensate material dispersion induced by the multiple optical components (a half wave plate, a thick polarizer and a lens) before the bulk fused silica, we intentionally give pre-chirp in the pulse which generates the SC continuum. The same pulse is used for the reference pulse which is gating the continuum and generating transient grating in the nonlinear medium.

When the input beam focuses down to bulk fused silica, the numerical aperture (NA) has a maximum value that can generate a stable SC. If the NA is 0.25 or higher, then the transparent bulk materials are damaged before generating any continuum. [50] In our setup, the numerical aperture is 0.01, which is less than the threshold of NAs for SC generation, using a lens of 250mm focal length. The input energy is controlled, with caution, by a combination of a half wave plate and a polarizer because too much power of the input pulse induces bulk damage and introduces a lot of spatial distortions in the beam, which can affect TG X FROG traces. The continuum is generated by sending ~3μJ of the pulse energy and 210 fs of the pulse duration, which is pre-chirped, through 12.5mm of bulk fused silica. Unlike SC generation in microstructure fibers, which is purely temporal, dynamical processes with the transverse mode characteristics, continuum in bulk materials is a highly complex process involving spatial and temporal effects. [45] As a result, the continuum has spatial structure in the beam even though we filter out the conical emission part. The continuum generated from the fused silica is collimated by a lens of 150mm focal length and passed through a Schott BG40 filter, which passes the visible and blocks the intense 800 nm portion of the spectrum due to the

spectrometer's limited dynamic range. This visible spectrum part of the continuum represents the asymmetric blue-broadening characteristic of the SC generation. [50]

On the other side, after the first beam splitter, the beam splits into two pump beams. Each pump beam has ~70μJ of pulse energy. The delays of the two pump beams are controlled by two translation stages in order to make the continuum and two pump beams overlapped, in time, in the nonlinear medium (ZnS).

Figure 3 – 6 shows the formation of transient grating in the nonlinear medium. Two pump beams intersect at an angle Θ at the nonlinear medium by the cylindrical lens and create an interference pattern. (In our experiment, we use cylindrical mirrors instead of a cylindrical lens. In the figure, it is conceptually easy to understand.) Then the interference pattern forms the refractive-index grating in the optical-Kerr medium, the index of refraction of which changes due to the intensity in the medium, when the two pump beams overlapped in time and space.

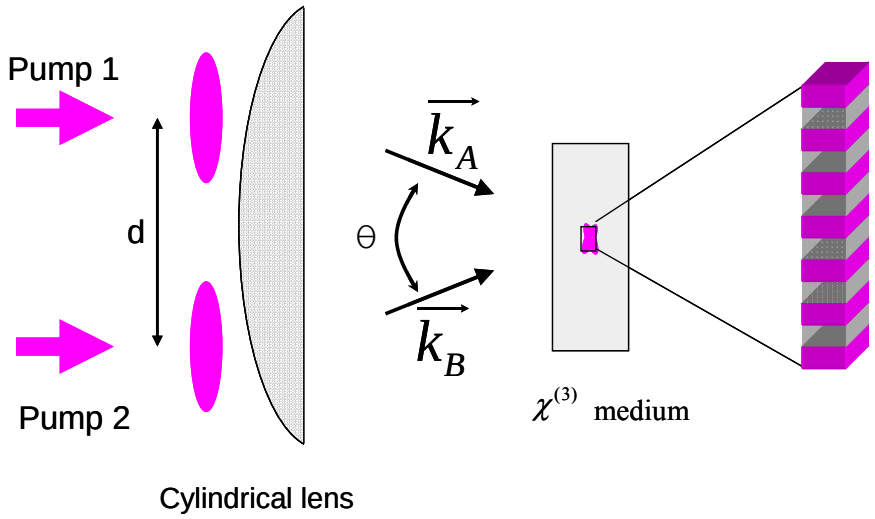

Figure 3 – 6: Formation of transient grating in a nonlinear medium. Two pumps focus and cross at an angle θ, and they make an interference pattern in the medium. The change of intensity in the medium induces a refractive-index grating.

The grating vector $\vec{q}$ is

$$\vec{q} = \pm(\overrightarrow{k_A} - \overrightarrow{k_B}) .$$

The above equation seems to have two places where the signal pulse emerges. However, the signal pulse emerges from the unique direction, if the two pump beams are well defined because only the minus first order of the transient grating can be seen. In the TG X FROG geometry, we use continuum (white-light) as a probe beam which has different wavelengths with the wavelengths of the two pump beams (800nm), and so it is trivial to find out which ones are the pump beams. In normal TG FROG, however, because three beams are identical and so each beam can be either a probe or a pump, it is not trivial to distinguish the probe beam from the pump beams. Actually, depending on which pulse is variable delay (with the other two coincident in time), the probe or the pump can be decided. As a result, the TG FROG trace is mathematically equivalent to PG FROG or SD FROG. We are going to talk about this in chapter 4 in detail.

The spatial period Λ of the pattern is

$$\Lambda = 2\pi / q ,$$

where $q = \left|\vec{q}\right|$.

Λ can be expressed in terms of the pump wavelength λ_p and the angle θ

$$\Lambda = \lambda_p / 2\sin(\theta / 2) .$$

The spatial period Λ is a function of the angle θ, a function of a separation d between two pump beams and a focal length of the cylindrical optics. In our experiment, in order to minimize the pulse distortions by cylindrical optics, the separation d is very small.

(Figure 3 – 6) As a result, the transient grating in the nonlinear medium has a relatively poor spectral resolution compared with a real grating.

In order to implement TG X FROG in a single-shot beam geometry to measure a few ps pulse, a cylindrical mirror of 125mm focal length focuses two pump beams and the continuum, and the two pumps and the continuum cross at a large angle (13.5 degree), generating ~11 ps delay range, shown in Figure 3 – 6. In TG FROG geometry, in order to avoid temporal smearing effects due to large beam angle, normally, we use a small angle (less than 5 degree). However, in our TG X FROG, a relatively large angle is permitted because the temporal resolution of the TG X FROG is bigger than the temporal smearing effects. In other word, in order to generate ~11ps delay range, the temporal resolution of the TG X FROG is about 100 fs, which is bigger than the geometrical time smearing effect, which is depending on the thickness of the nonlinear medium and the crossing angle between two pumps and continuum.

The relative delay between the pumps and the continuum varies with position at the ZnS nonlinear medium. For a nonlinear medium, a ZnS crystal (3mm thick) is used because this material has a relatively high third-order nonlinear optical coefficient and is transparent from 380nm to 1100nm, covering the whole continuum spectrum.

The continuum is overlapped and crossed in the nonlinear medium and diffracted by the grating induced by the two pumps to produce the signal pulse. Figure 3 – 7 shows that two pump beams overlap in time and space completely and generate transient grating in the in the nonlinear medium. Then the continuum is crossed with the induced grating in the medium and diffracted by the grating. The maximum delay range by the TG X FROG is a function of the crossing angle Θ between the pumps and continuum and beam

sizes of the pump beam. Note that, in Figure 3 – 7, the continuum, a long pulse, is overlapped and crossed with the two pumps, short pulses, in the medium. A slice of the transient grating generated by the two pumps is gating the continuum for each delay. As a result, the different delay in the continuum is corresponding to the different position.

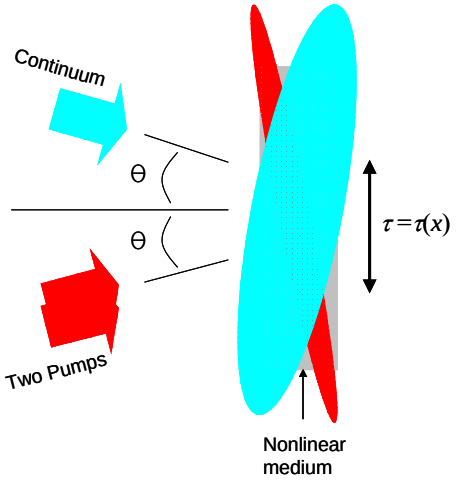

Figure 3 – 7: Schematic of three pulses (two pumps (red) and continuum (blue)) for a single-shot TG X FROG geometry. The continuum and two pumps cross at an angle Θ, mapping delay onto transverse position. The two pumps are overlapped in time and space and form a transient grating in the nonlinear medium. The continuum is diffracted by the transient grating.

Figure 3 shows the phase-matching condition for our TG X FROG. In general, in TG FROG, the three input beams have the same frequency, and are arranged so that, on a card, they appear to be on three corners of a rectangle, or a square. [Fig. 3 – 8 (a)] As a result, this geometry automatically satisfies the Bragg condition, or phase-matching condition, independent of the input wavelength. [Fig. 3 – 8 (b)] However, when

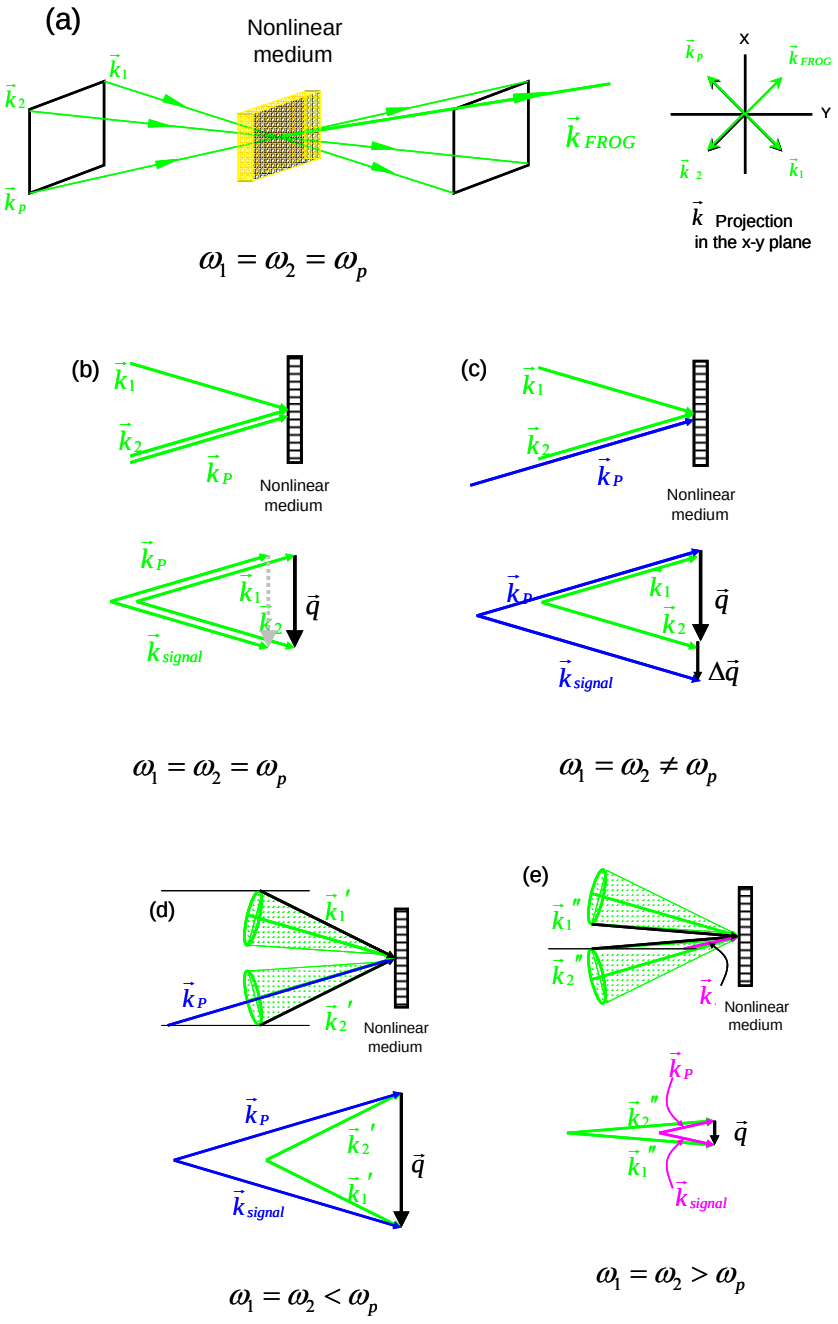

Figure 3 – 8: Phase-matching condition for the TG X FROG. (a) K-vector diagram for TG FROG phase-matching. K_1 and K_2 are the two pumps. K_p is the probe beam to be measured. K_{FROG} is the FROG signal. The signal beam emerges from the other corner of a rectangle of the three input-beam geometry. The phase-matching

condition is $K_{FROG} = K_1-K_2+K_3$. (b) The Bragg condition for the TG FROG, where $W_1= W_2 =W_p$. (c) When $W_1= W_2 \neq W_p$, the Bragg condition is not satisfied, where $\Delta\vec{q}$ is the phase-mismatch. (d) The Bragg condition for the blue side of the continuum and (e) the Bragg condition for the red side of the continuum when we use the focused pump beams.

measuring the continuum, the center wavelength of the continuum, or the probe, is not the same with the one of the pump beams. In this case, there is a phase-mismatch $\Delta\vec{q}$ because these three beams can not satisfy the Bragg condition. [Fig. 3 – 8 (c)] Therefore, it is clear that the total phase-matching bandwidth is comparable with the bandwidth of the pump beams. In our TG X FROG, however, because the two pump beams focus into the nonlinear medium (ZnS), the k-vectors can change even if they have the same frequency. [Fig. 3 – 8 (d) and (e)] These different k-vectors in the pump beams (at 800nm) can phase-match the k-vector in the blue side of the continuum (at 550nm). [Fig. 3 – 8 (d)] Similarly, they can phase-match the red side of the continuum. [Fig. 3 – 8 (e)] As a result, the total phase-matching bandwidth of the TG X FROG is a function of the beam size of the pump beam, the crossing angle of the two pump beams and the focal length of the cylindrical mirror. Accordingly, the arrangement can phase-match from 380nm to 1600nm when using the pump beam diameter of 7mm and the crossing angle of 4.6°. If the smaller focal length of the cylindrical lens and the bigger beam size are used, the total phase-matching bandwidth of the arrangement increases.

The signal beam is sent to an image spectrometer with a 150g/mm groove density and 500nm blaze angle grating. When sending the signal to the spectrometer, in order to maintain delay information in the medium, we use an imaging lens for imaging from the nonlinear medium to the entrance slit in the spectrometer. The signal beam,

entered in the spectrometer, is collimated by a concave mirror, the collimated beam impinges the grating, with 150g/mm, and a camera can capture a spectrally resolved TG X FROG trace by another concave mirror. The camera has two-dimension array. One is delay axis τ running vertically while the other is wavelength axis running horizontally. In order to calibrate the wavelength axis, we use a calibration lamp with characteristic peaks in certain wavelengths. For the delay axis calibration, we use a 1mm-thickness piece of glass, which corresponds to certain amount of delay. If we record the change of the position in the camera when we put the piece of glass, we can calibrate the delay axis.

Our measured TG X FROG trace has dimensions 640 x 512, which we interpolate and expand to 2048 x 2048 for retrieval. In our setup, the TG X FROG trace is mathematically equivalent to polarization-gate (PG) X FROG [51], because, like PG FROG, the pumps generates the transient grating, depending on the relative intensity difference generated by the interference pattern.

PG X FROG, or TG X FROG, code is similar to the SFG X FROG code. Only difference between two codes is the gate function. The electric field of the TG X FROG signal beam has the form

$$E_{sig}^{TG}(t,\tau) = E(t)\left|E_{ref}(t-\tau)\right|^2,$$

and the TG X FROG trace has the form

$$I_{sig}^{TG}(\omega,\tau) = \left|\int_{-\infty}^{\infty} E(t)\left|E_{ref}(t-\tau)\right|^2 e^{-i\omega t}dt\right|^2.$$

For retrieving the TG X FROG trace, we use an iterative Fast Fourier-transform (FFT) algorithm with general projection. Figure 3 - 9 shows a flow chart of the TG X FROG algorithm. TG X FROG algorithm needs the experimentally measured TG X FROG trace

($I_{TGXFROG}(\omega_i, \tau_i)$) and the retrieved electric field of the reference pulse as an input data. The algorithm begins with an initial guess for the electric field of the continuum and calculates the corresponding signal field, $E_{sig}^{TG}(t_i, \tau_i)$. Since the TG X FROG trace is a function of ω and τ, the algorithm Fourier-transforms, or Fast-Fourier-transform (FFT) $E_{sig}^{TG}(t_i, \tau_i)$ with respect to t_i in order to obtain $\tilde{E}_{sig}^{TG}(\omega_i, \tau_i)$. By the general projection, the algorithm modifies the electric field from $\tilde{E}_{sig}^{TG}(\omega_i, \tau_i)$ to $\tilde{E}_{sig}^{\prime TG}(\omega_i, \tau_i)$, and after this modification, by inverse Fast-Fourier-transform (IFFT), $\tilde{E}_{sig}^{\prime TG}(\omega_i, \tau_i)$ transforms to $E_{sig}^{\prime TG}(t_i, \tau_i)$. Now, $E_{sig}^{\prime TG}(t_i, \tau_i)$ replaces $E_{sig}^{TG}(t_i, \tau_i)$. The algorithm keeps changing the electric field of the continuum, minimizing Z which is one useful distance metric Z. The distance metric Z has the form

$$Z = \sum_{i,j=1}^{N} \left| E_{sig}^{\prime TG}(t_i, \tau_j) - E(t_i) \left| E_{ref}(t_i - \tau_j) \right|^2 \right|^2 .$$

The reference pulse remains unchanged during the generalized projection. In order to measure the progress of the algorithm, we use the FROG error G also used by other FROG geometry.

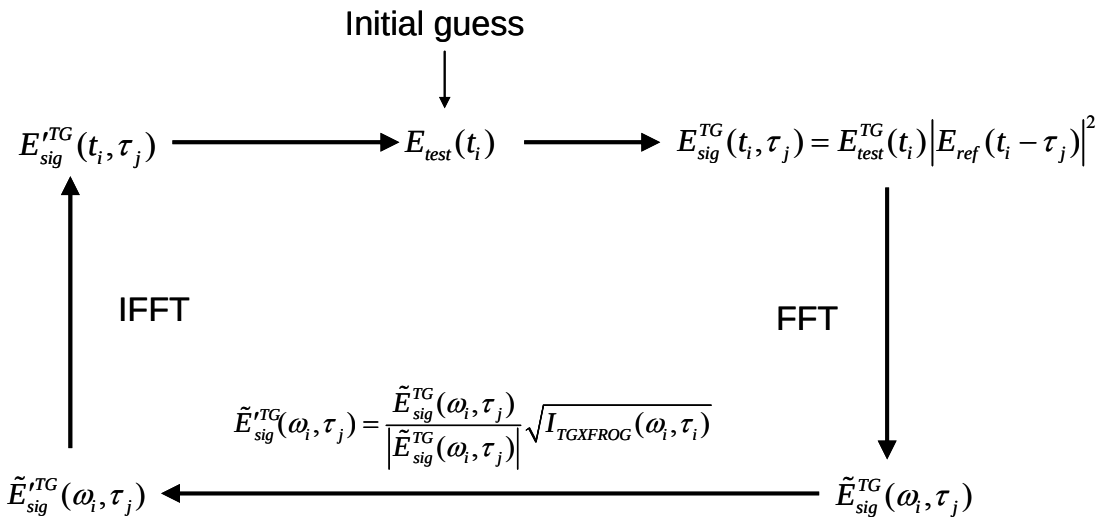

Figure 3 – 9: Schematic of the TG X FROG algorithm. In the beginning, the initial guess is arbitrary. We use a random initial guess. The initial guess is modified by the measured trace, minimizing Z. The algorithm keeps doing this until getting a small FROG error.

The PG X FROG, or TG X FROG, code retrieves intensity and phase of the pulse from the measured trace in Figure 3 – 10 and Figure 3 – 11. In the measured trace, we can not see any soliton formation, unlike other continuum from microstructure fibers. The slope of TG X FROG trace corresponds to the temporal chirp, as the slope of TG FROG trace does. After retrieving the measured trace, we can see fine structure in the retrieved trace. Since the retrieved trace reveals the fine structure which we couldn't see in the measure trace, the agreement between the measured trace and the retrieved trace wasn't good.

The retrieved temporal phase is mainly quadratic, in agreement with the slope of the TG FROG trace. [8, 11] We observe fine structure in the retrieved trace and spectrum that we couldn't see in the measured trace. The fine structure, revealed after retrieving the measured traces, was reported by X. Gu et. al. in 2002, using a multi-shot sum frequency

generation cross correlation FROG measurements generated from 152cm microstructure-fiber. [47]

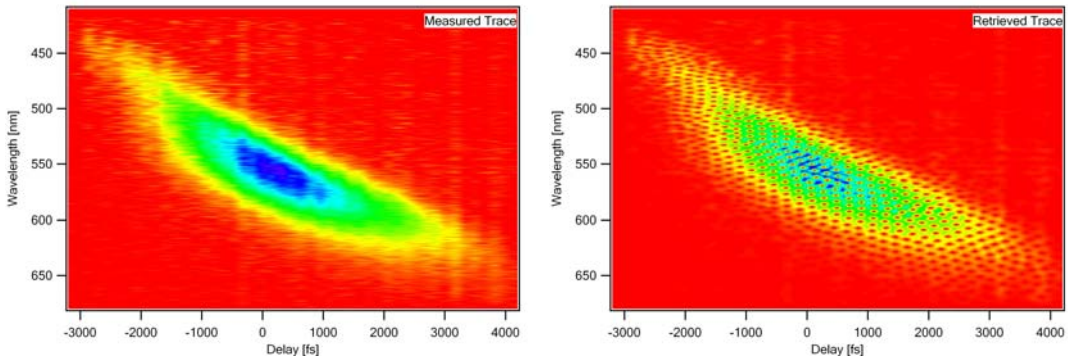

Figure 3 – 10: Measured (left) and retrieved (right) TG X FROG traces for the measurement of the continuum from a 12.5mm bulk fused silica.

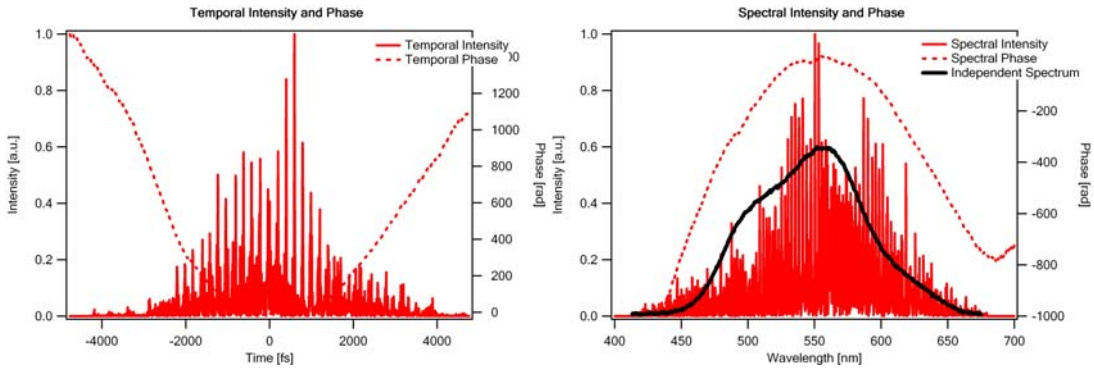

Figure 3 – 11: Left: The temporal intensity and phase measured using TG X FROG. Right: Retrieved spectral intensity and phase of the continuum pulse measured using TG X FROG and the independent spectrum for comparison.

Like the SC from the microstructure-fiber, the explanation for the fine structure after retrieving is that information washed out in one domain remains in the other domain. The resolution of the time domain, in our experiment, is poor (~100fs) because, in order to achieve a single- shot FROG geometry, a camera should cover a long delay

range (~11-ps) to measure 8-ps pulses. While the fine structure in time domain is smeared out, the information, in the trace, in the other domain can reconstruct the fine structure in the pulse because FROG traces contain much redundancy. In the independent spectrum measurement, unlike continuum from the microstructure-fiber, we can't see fine structures because the spatial chirp in the beam smears out fine structures.

3. 4 Conclusions

We demonstrate a single-shot measurement technique for continuum generated from a bulk fused silica. Right now, this method is used for continuum generated from bulk materials because we use the third-order nonlinear-optical beam geometry, requiring high peak energy for continuum. However, we believe that this method can be used for SC generated from microstructure fibers and any other continuum when energy of pump beams is strong enough.

Since the first invention of FROG based on SHG, many ultrafast scientists have been using SHG-FROG for characterizing their pulses and it is no doubt that the most sensitive version of FROG is the SHG FROG and it is quite successful. After this invention, other ultrafast-laser-pulse measurement devices were invented. One of them is the spectral phase interferometry for direct electric-field reconstruction, using self-referencing interferometric technique. We call it SPIDER. This device, also, uses SHG process. Therefore, we can say that most of ultrafast-laser-pulse devices are based on SHG process even though other optical nonlinear processes, such as third nonlinear optical properties, are only occasionally used for pulse measurement.

One of reasons that we usually use SHG is that the beam energy is not strong enough to use third nonlinearity. However, in these days, many research groups have high power laser sources, like generatively chirped-pulse-amplifiers (CPA), and they should be able to use third nonlinearity for measuring their pulse. Besides, pulses from the amplifiers are very complex and vary shot-to-shot because they undergo high nonlinear process to maximize the power of the pulses. In addition to this, some of them are very short pulses, requiring an extremely thin SHG crystal which is not available now, when we try to measure the pulses using SHG-FROG or other measurement devices based on SHG process.

Another reason is that after the invention of FROG, research for the other FROGs using third optical nonlinearity has not been done properly because SHG-FROG could manage to measure most of pulses not only from the oscillator but also from amplifiers. However, we believe that in near future, the ultrafast pulse measurement field needs a new powerful device, which can measure a very short pulse with an extremely broaden bandwidth, the TG X FROG, avoiding strict phase-matching condition in pulse measurement techniques based on SHG process.

CHAPTER 4

EXPERIMENTALLY SIMPLE, EXTREMELY BROADBAND TRANSIENT-GRATING FREQUENCY-RESOLVED-OPTICAL-GATING DEVICE

This chapter originally appeared as a paper by the author:

Dongjoo Lee, Selcuk Akturk, Pablo Gabolde and Rick Trebino, "Experimentally Simple, Extremely Broadband Transient-Grating Frequency-Resolved-Optical-Gating Device", Optics Express 15, 2007, 760-766

4. 1 INTRODUCTION

Despite recent great advances in ultrashort-pulse measurement techniques, much remains to be done. In particular, these devices have relatively small wavelength-tuning ranges, and most are experimentally complex and difficult to align, especially when operating at odd wavelengths. Second-harmonic generation (SHG), the basis of most techniques, has a relatively stringent phase-matching requirement, so, even with angle-tuning, SHG-based devices can operate over only a few hundred nm in the near-IR and less in the visible and they require angle-tuning when the wavelength is tuned. In addition, SHG of UV wavelengths is not possible because SHG crystals are opaque at the second harmonic (< 200 nm). With regard to complexity, pulse-measurement devices generally require overlapping two or more beams in space and time, scanning the relative delay, and satisfying the phase-matching condition. Even newly proposed techniques operating at *common* (near-IR) wavelengths are often extremely complex and difficult to work with,

involving precisely collinear beams, interferometers, and/or pulse stretchers, and as many as a dozen sensitive alignment parameters.

Recently, we developed a technique based on the SHG frequency-resolved-optical-gating (FROG) method, which *is* extremely simple and which requires no alignment, except for angle-tuning the wavelength. Called GRating-Eliminated No-nonsense Observation of Ultrashort Incident Laser Light E-fields (GRENOUILLE) [53], it involves replacing the beam-splitter, delay line, and beam-combining optics with a single optical component called a Fresnel biprism, which simplifies the device tremendously. GRENOUILLE is also inexpensive and simple to use. It has also been quite successful at measuring visible and IR pulses over a wide range of pulse lengths, energies, and repetition rates [6, 7]. Unfortunately, GRENOUILLE, like all SHG-based pulse-measurement devices, has a limited wavelength range and cannot operate in the UV.

As a result, a given GRENOUILLE can only measure a fraction of the wavelength range of a particularly broadband device used in many laboratories, the optical parametric amplifier (OPA). The OPA's range is even broader when harmonic generation is also performed. Even excluding the UV range, measuring OPA pulses over the remaining OPA tuning range requires several SHG-based devices. In addition, due to the complexity of OPAs, OPA pulses also tend to suffer from beam wander and a host of other alignment issues, which calls, not only for a broadband device, but also for an ultra-simple, easily aligned one, insensitive to such effects as beam wander.

4. 2 BROADBAND SIMPLIFIED TG FROG

We present such a device here. In order to achieve broadband operation, especially in the UV, a third-order nonlinear-optical beam geometry such as self-diffraction (Figure 4 – 2), polarization gating (Figure 4 – 1), or transient grating (Figure 4 – 3) is required [53, 54].

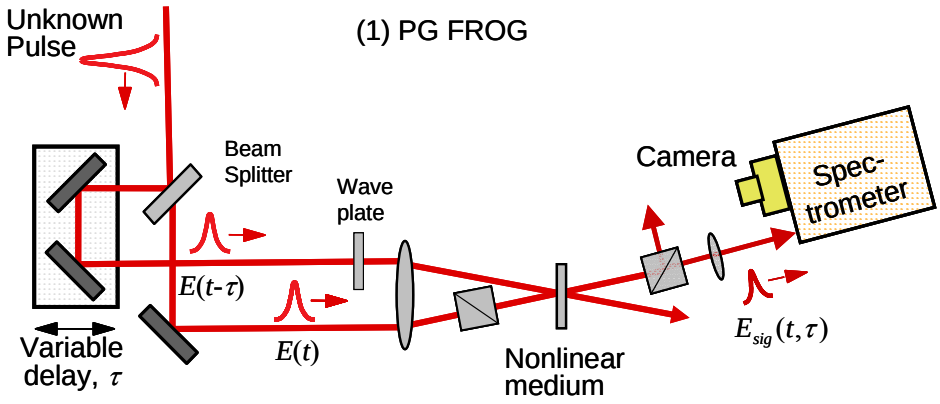

Figure 4 – 1: Polarization-gate (PG) FROG apparatus.

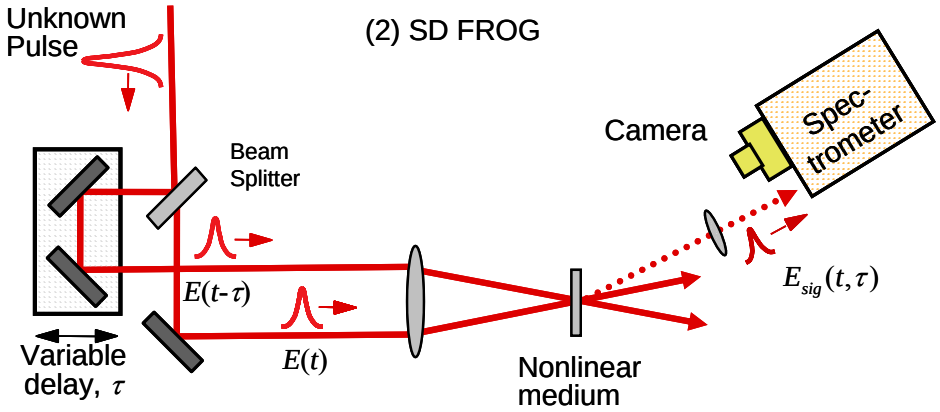

Figure 4 – 2: Self-diffraction (SD) FROG apparatus.

In PG FROG geometry, the unknown pulse is split into two. In order to get a 45 degrees linear polarization with respect to that of the probe pulse, one pulse (the gate pulse) is sent through a half-wave plate. The other (the probe pulse) is sent through polarizers. The

two pulses are spatially (and temporally) overlapped in a nonlinear medium such as a piece of fused silica. The nonlinear medium acts as a wave plate when the gate pulse is overlapped temporally, rotating the polarization of the probe pulse slightly. This allows some light to be transmitted through the other polarizer because birefringence occurs only if the gate pulse is present. Then a PG FROG trace, which is a spectrally resolved trace generated by the transmitted light and the second polarizer, is measured. The PG FROG trace is given by:

$$I_{FROG}^{PG}(\omega,\tau) \quad = \quad \left| \int_{-\infty}^{\infty} E(t)\left|E(t-\tau)\right|^2 \exp(-i\omega t)\,dt \right|^2 \tag{4-1}$$

In SD FROG geometry, the two pulses generate a sinusoidal intensity pattern and induced a material grating in a nonlinear material, which diffracts each pulse into the direction. As a result, the SD FROG trace can be measured in the left side and the right side of the two pulses after the nonlinear medium and they are identical. After a spectrometer, a camera can capture a SD FROG trace, which is spectrally resolved and is a function of delay. The SD FROG trace is given by:

$$I_{FROG}^{SD}(\omega,\tau) \quad = \quad \left| \int_{-\infty}^{\infty} E(t)^2 E(t-\tau) \exp(-i\omega t)\,dt \right|^2 \tag{4-2}$$

Unlike PG FROG, because SD FROG does not require polarizes, for which high extinction efficiency polarizes are unavailable in deep UV, it can be used for deep UV pulses. However, SD FROG is not a phase-matched process. As a result, in order to minimize the phase mismatch, the thickness of the nonlinear medium should be less than 200 μm and the angle between the two beams should be less than 2 degree.

The most versatile, sensitive, and accurate of these is the transient-grating (TG) geometry. However, the TG beam geometry is also the most complex, requiring splitting the pulse into *three* pulses in separate beams, and crossing two of them in space and time to generate a transient grating in a $\chi^{(3)}$ medium that is probed by the third beam, which itself must be carefully aligned (Figure 4 – 3).

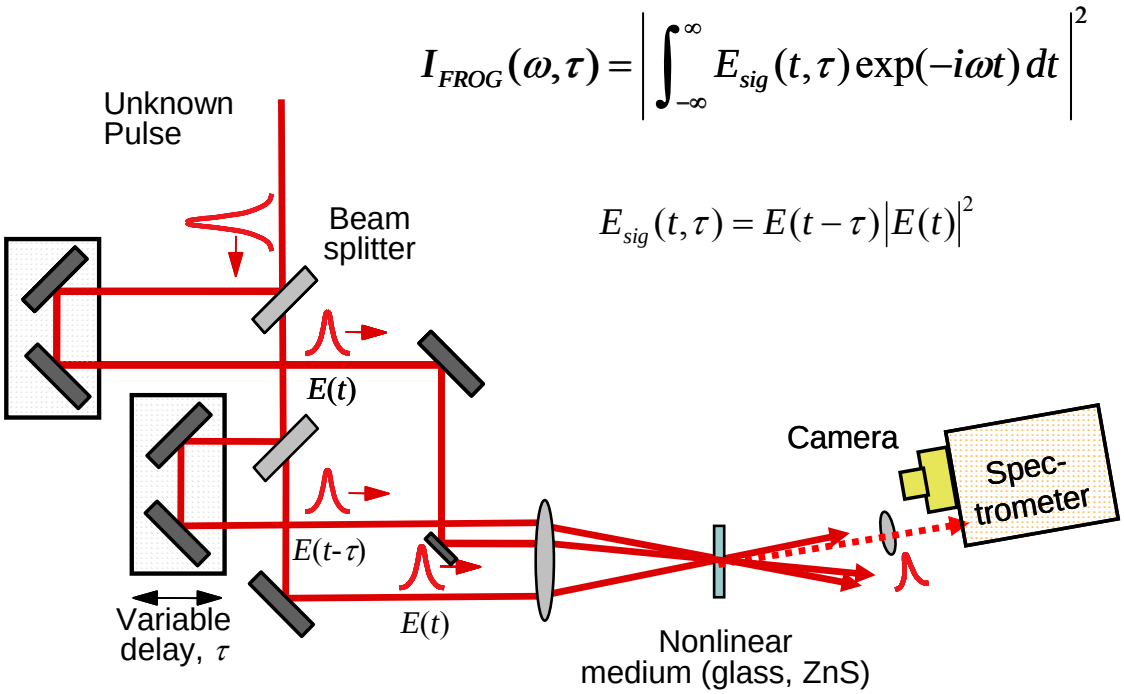

Figure 4 – 3: Transient grating (TG) FROG apparatus.

In TG geometry, the unknown pulse is split into three pulses. Two of them are overlapped in time and space in the nonlinear medium (a piece of fused silica or ZnS), generating a refractive index grating. The third beam (the probe) is diffracted by the induced transient grating and the signal emerges from another corner of a rectangle of the three beam geometry. The signal is sent to a spectrometer and then the spectrally resolved TG FROG trace is captured by a camera.

TG FROG has several advantages when comparing with the other FROG geometries using a third order nonlinearity. Unlike PG FROG, TG FROG doesn't use any polarizers which are normally thick, introduce pulse distortions, and are not available in deep UV. In addition, TG FROG uses a background-free geometry. In PG FROG, the efficiency of the polarizer is very important because we are supposed to measure polarizer-leakage by a birefringence through the electric Kerr effect. However when the wavelength decreases, the extinction efficiency of the polarizers decreases. PG FROG geometry is not suitable for UV pulse measurement because the extinction efficiency of the polarizers in UV region is poor.

Unlike SD FROG, TG FROG can be phase-matched automatically. Because SD FROG is not phase-matched process, this only allows us to use a very thin crystal, reducing the sensitivity of the device, and a very small angle between two beams, generating scattered-light background. However, in TG FROG geometry, we can use a thick crystal, enhancing signal strength due to the length-squared dependence of the signal, as a third order nonlinear medium. In addition, larger beam angles may be used that in SD FROG, reducing scattering-light background. More importantly, using the diagonal element of the susceptibility tensor makes TG FROG significantly more sensitive than other third order geometries, because the diagonal element of the susceptibility tensor is a factor of three larger than off-diagonal elements used in PG FROG and SD FROG. As I mention before, SHG FROG is the most sensitive but there is no second harmonic crystal for UV pulses. As a result, TG FROG is the best option for measuring UV ultrafast pulses.

If a TG FROG is desired, the diffracted four-wave-mixing output pulse must then be spectrally resolved vs. delay [54]. As a result, this powerful beam geometry is only occasionally used for pulse measurement. [54] So, in this work, we significantly simplify TG FROG in the spirit of GRENOUILLE, so that it has no sensitive alignment parameters. The resulting device is very easy to set up, is essentially automatically aligned, is inherently extremely broadband, and operates well in the UV. Even better, it is automatically phase-matched for all wavelengths and so does not require re-alignment if the wavelength is tuned. A single such simplified TG FROG device can operate from the UV to the IR with no change of optics or realignment. Like GRENOUILLE, it naturally operates on a single-shot basis. While not currently suitable for measuring pulses from nJ-per-pulse oscillators, it is suitable for measuring microjoule- or higher-energy pulses from a high-power or amplified system or OPA. It also yields a sensitive measurement of the pulse-front tilt, very useful for OPAs, which often also suffer from this distortion.

Figure 4 - 4 schematically shows the device. The input beam is split into three beams by a simple mask with three holes. A cylindrical lens focuses the beams to lines in the $\chi^{(3)}$ medium. In the other dimension, a Fresnel biprism crosses the beams in space and time. The angle between the line-focused beams maps delay onto position, so that the relative delay need not be scanned, as long as the crossed beams are imaged onto and spatially resolved by the camera. Two of the beams overlap perfectly in space and time across the glass medium and form a transient grating. The other beam crosses the grating at an angle, and thus varies the relative delay, τ, between the pulses transversely in space. The diffracted signal pulse, which emerges from the interaction region as the fourth beam in the rectangle formed by the three input pulses, is spectrally resolved by a simple

grating/lens spectrometer, in which the line focus in the nonlinear medium acts as the entrance slit.

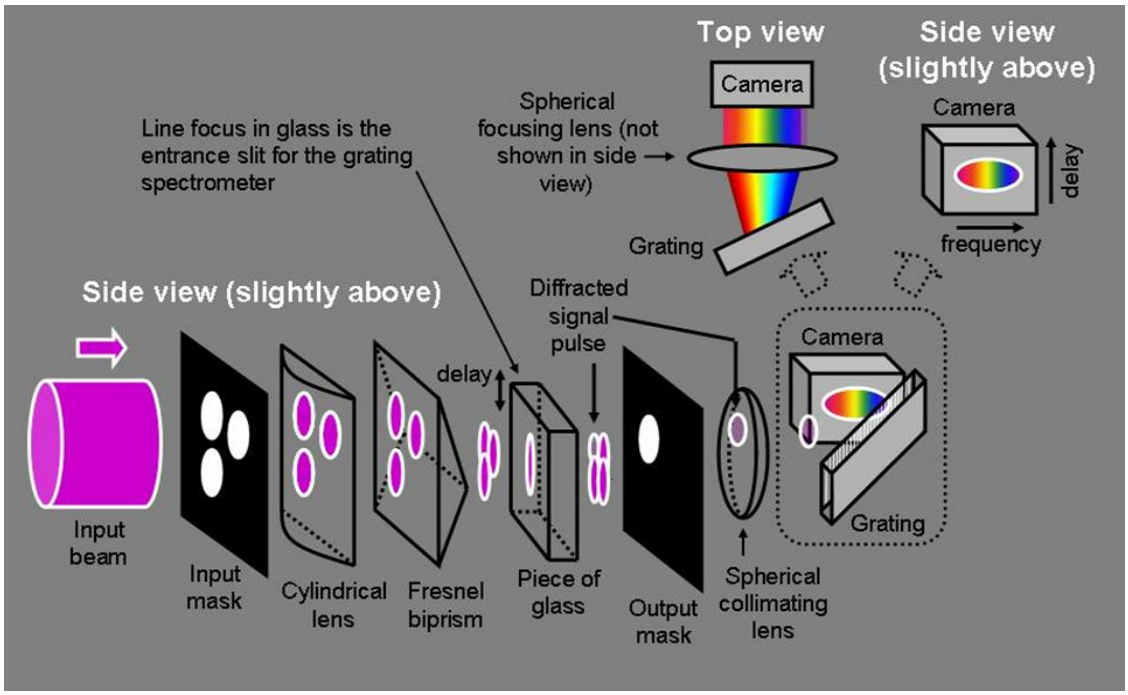

Figure 4 – 4: Simple broadband TG FROG device. The input mask splits the input beam into three beams, which are then overlapped in the $\chi^{(3)}$ medium (ZnS in these initial measurements, but fused silica in a more broadband device that includes the UV). The cylindrical lens yields line foci, mapping the delay onto transverse (vertical) position, allowing single-shot measurement. The upper two beams cross and form a transient grating in the crystal. The lower beam is diffracted by the transient grating and generates an autocorrelation signal beam in the other corner of the rectangle. The line focus then acts as the entrance slit to a home-made spectrometer consisting of a collimating lens, diffraction grating, and focusing lens, yielding a single-shot TG FROG trace with delay running vertically and wavelength horizontally.

The signal field in TG FROG is: $E_{sig}(t,\tau)=E_1(t)E_2(t)*E_3(t-\tau)$ where $E_i(t)$ is the i^{th} input pulse. In our device, the TG FROG trace is mathematically equivalent to polarization-gate (PG) FROG, a highly intuitive version of FROG. Because pulse #3 is crossed at an angle to the other two pulses, it is variably delayed, and the signal pulse is given by [20, 54]:

$$I_{FROG}^{TG}(\omega,\tau) \quad = \quad \left| \int_{-\infty}^{\infty} E_1(t)E_2^*(t)E_3(t-\tau)\exp(-i\omega t)\,dt \right|^2 \tag{4-3}$$

Because all pulses are identical, this becomes:

$$I_{FROG}^{TG}(\omega,\tau) \quad = \quad \left| \int_{-\infty}^{\infty} |E(t)|^2 E(t-\tau)\exp(-i\omega t)\,dt \right|^2 \tag{4-4}$$

where we have performed a simple change of variables to yield the desired result. This is just the expression for the PG FROG signal field.

4. 3 DEVICES

In our device, the input beam was expanded by a 4x telescope (not shown) and was then split by an input mask into three beams as in Figure 4 – 4, as demonstrated previously by M. Li and coworkers [55]. Our input mask consists of three holes which are rectangular in shape (10 mm x 2 mm). Two of the beams were overlapped in space and time at the third-order nonlinear material by a cylindrical lens, producing a line-shaped transient refractive-index grating (with vertical fringes). The third beam was overlapped and crossed with the others by the Fresnel biprism. Diffraction by the induced-grating produces the signal pulse. For the third-order nonlinear material, we used a 3-mm-thick ZnS crystal, which is transparent from 370 nm to 14 μm. Fused silica can be used for

broader-band (UV, visible, and IR) operation, albeit with somewhat less device sensitivity at the longer wavelengths. Our device also included a simple imaging spectrometer, whose entrance slit comprised the line focus in the crystal. The signal was isolated by an output mask, collimated by a spherical lens, and diffracted off a 1200-line/mm groove-density grating. After a spherical focusing lens, a spectral resolved TG-FROG trace resulted on the CCD camera, in which the delay varied vertically and frequency varied horizontally (Figure 4 – 4).

The focal length of the cylindrical lens was 50 mm. The Fresnel biprism had an apex angle of 160°, yielding a delay range of 5 ps [54]. The crossing angle of the two pump beams was about 5.2°, resulting in a transient grating with a ~ 9 μm spatial period when the wavelength is 800 nm [56]. The use of a relatively thick crystal (3 mm) is permitted because the transient-grating process is automatically phase-matched, [56].

4. 4 EXPERIMENTS

We demonstrated our device for both 800-nm and 400-nm pulses with no change of any components between the two measurements. We first describe our measurements of 800-nm pulses, which were from a Ti:Sapphire regen and were ~150-fs long, 500 μJ in energy, and at a 1-kHz-rep-rate. Figure 4 – 5 shows the measured and retrieved traces, and the agreement is very good. The FROG error for the 128×128 traces was about 0.57%.

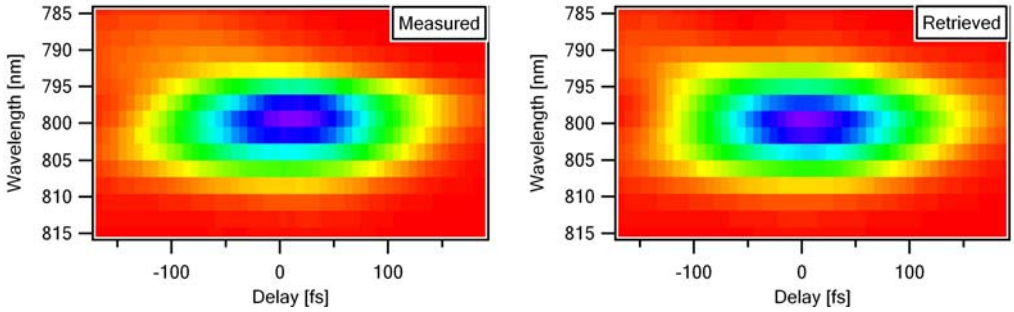

Figure 4 – 5: Measured (left) and retrieved (right) TG FROG traces for our 800-nm pulse measurement.

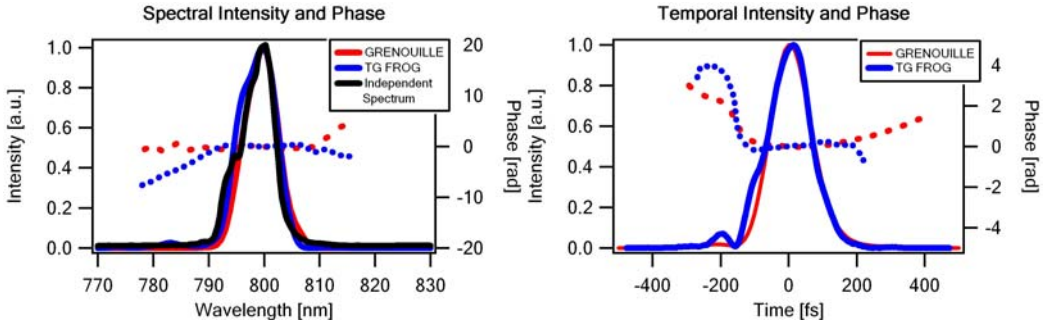

Figure 4 – 6: Retrieved intensity and phase of the pulse using the simplified TG FROG (and GRENOUILLE and independent spectrum for comparison). On the left are the spectral intensity and phase; on the right are the temporal intensity and phase.

To verify the accuracy of our measurement, we also measured the pulse using a commercial GRENOUILLE from Swamp Optics (Model 8-50) and a commercial spectrometer from Ocean Optics (USB 2000). Figure 4 – 6 shows these results, and the agreement is good. The pulse's measured FWHM duration and bandwidth that TG-FROG retrieved are 140 fs and 8.3 nm respectively. GRENOUILLE measured a 139 fs pulse in comparison. In the retrieved spectral intensity, the GRENOUIILLE lacked the resolution to see the finest spectral structure of the pulse, which our TG FROG (whose grating spectrometer had higher resolution) could. This causes the minor discrepancy between GRENOUILLE and TG FROG measurements.

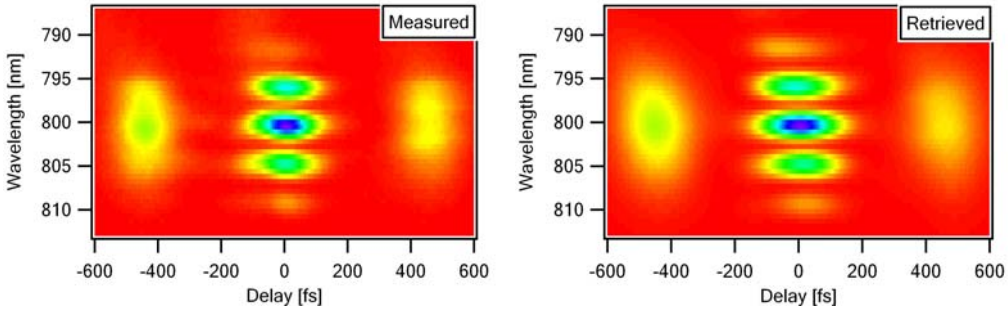

Figure 4 – 7: Measured (left) and retrieved (right) TG FROG traces for a double pulse.

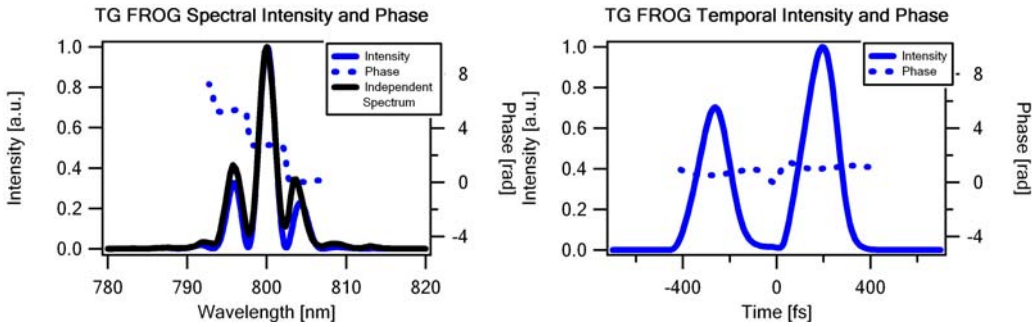

Figure 4 – 8: Left: The retrieved spectral intensity and phase of a double pulse measured using TG FROG and the independent spectrum for comparison. Right: The temporal intensity and phase measured using TG FROG.

In order to test the device's ability to measure complicated pulses, we measured a double pulse generated by a Michelson interferometer using the same device. Because the effective size of the beams generated by the holes in the input mask was ~10mm, this setup yielded a sufficient delay range (~5 ps) to measure a 1 ps long double pulse using the same 160°-apex-angle Fresnel biprism. These beams were overlapped at the focus of the cylindrical lens in the piece of ZnS, yielding the characteristic double-pulse TG FROG trace shown in Figure 4 – 7. The agreement between the measured and retrieved traces (Figure 4 – 6) was good. The FROG error for the 512×512 traces was about 0.36%. The retrieved intensity and phase of the pulse are shown in Figure 4 – 8. To verify the measured pulse, whose time-bandwidth product was too large to be measured with

any commercially available device, we also measured the spectrum with a commercial spectrometer (Ocean Optics USB 2000), also shown in Figure 4 – 8, and the agreement is good.

With the same device (no optics were changed), we also measured a 400-nm pulse, generated by second-harmonic generation of the amplified Ti:Sapphire pulses using a 500-μm type-I BBO crystal. The output of the regenerative amplifier was ~ 520mW at 800 nm, and the output of the second-harmonic generation was ~ 85mW (conversion efficiency ~ 16%).

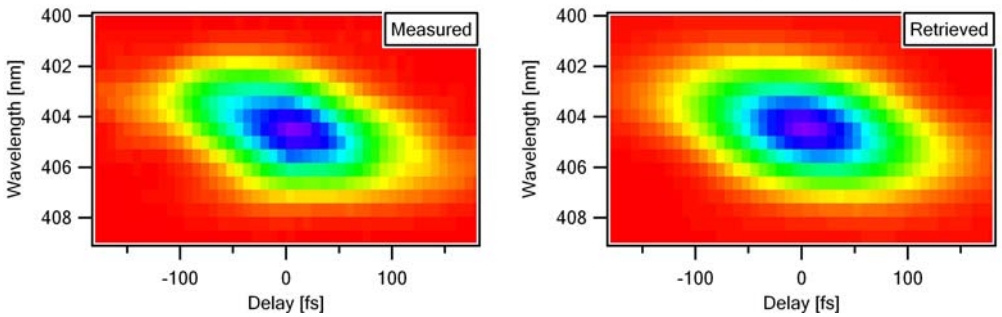

Figure 4 – 9: Measured (left) and retrieved (right) TG FROG traces for the measurement of a 400-nm pulse.

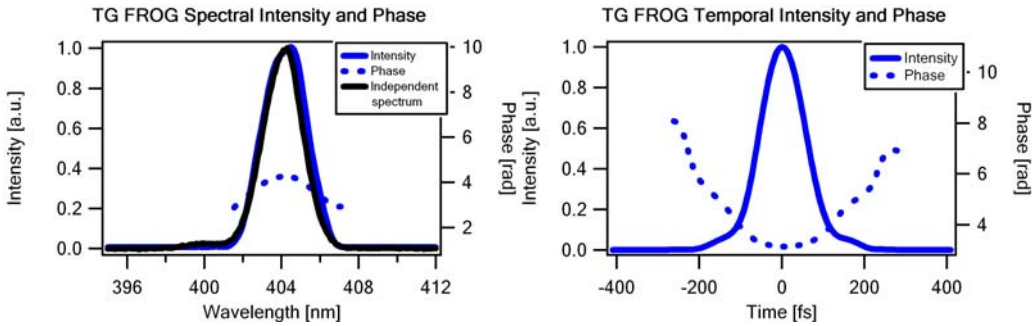

Figure 4 – 10: Left: Retrieved spectral intensity and phase of a 400-nm pulse measured using TG FROG and the independent spectrum for comparison. Right: The temporal intensity and phase measured using TG FROG.

The generated UV pulse was sent to the TG FROG device, which measured the 800-nm pulses above. The only realignment required in our TG FROG in order to measure this pulse was to change the grating angle in order for the 400-nm signal to impinge on the camera.

Figure 4 – 9 shows the measured and retrieved traces for the 400-nm pulse. The FROG error for the 128×128 traces was about 0.40%. The retrieved intensity and phase of the pulse are shown in Figure 4 – 10. To verify the measured pulse, we also measured the spectrum with a commercial spectrometer (Ocean Optics USB 4000), also shown in Figure 4 – 10, and the agreement is good. The pulse's FWHM duration and bandwidth retrieved by TG-FROG are 130fs and 2.6 nm, respectively. In order to minimize the group velocity dispersion, we used optics made of fused silica because fused silica is less dispersive than BK7 in the 400 nm region. The temporal distortion introduced by the small amount of fused silica in the TG FROG device (~ 5 mm thickness fused silica for the cylindrical lens and the Fresnel biprism) is negligible, compared with the pulse's FWHM.

An experimental issue worth mentioning is that, even though TG FROG enjoys a background-free signal because the signal propagates in a unique direction, stray light can still be a problem because the signal pulse is of the same wavelength and polarization as the stronger input beams. However, placing the output mask in the image plane of the input mask by the cylindrical lens effectively removes most of this stray light. Also, using a small slit after the collimating lens further helps to reduce the stray light. As a result, the device can be compact and can also achieve a good signal-to-noise ratio.

Ideally, TG FROG is the one that is both phase-matched and free of thick materials, such as polarizers. However, the price of these advantages is complexity because TG FROG requires three replicas from the input beam, using two beam splitters. Once we use beam splitters, it is necessary to use variable delay moving stages in order to make them overlapped in time. Eventually, we need to make the three replicas overlapped in time and in space, which introduces six sensitive alignment degrees of freedom (four spatial and two temporal). In order to avoid the complexity, we introduce a way to use an input mask. On the other hand, using an input mask may cause bad spatial profile of the three replicas when the input beam size is not expanded enough.

One might ask whether we actually needed the diffraction grating spectrometer the device. After all, the GRENOUILLE technique uses the angular dispersion of the SHG phase-matching condition of the nonlinear medium and so the SHG crystal acts as its own spectrometer. Analogously, here we actually induce a *grating* in the nonlinear medium, so why not use it for spectral resolution? Indeed, the induced grating would even diffract the beam in the desired direction, perpendicular to the delay direction, just as in GRENOUILLE. The problem, however, is that the number of fringes here is so small that the resolution of this grating is too poor to resolve the pulses of interest. On the other hand, for beams of very high energy, for which focusing is not necessary to achieve a strong TG signal, a larger spot size at the nonlinear medium should make a true "TG GRENOUILLE" possible.

In principle, our TG FROG device operates from the UV to the IR. In our particular device, the camera's response limited the operating range to 380 nm to 1100 nm. As a result, our particular device can operate over a spectral range of 720 nm from

the near-UV to near-IR. A more broadband camera could achieve a larger operating range.

4. 5 ANOTHER WAY TO GENERATE THREE REPLICAS

If we want to use a TG FROG geometry, handling three beams are always problematic. One issue for handling three beams is generating three replicas using two beam splitters. Once these beam splitters split the input beam into three beams, and then they need to be overlapped in time and space to order to generate FROG signals. This is hard and can introduce pulse distortions during aligning the optics. We use a simple input mask to generate three input beams. Here we demonstrate another simple way to generate three replicas from the input beam without spatial profile distortions using a 2D low density transmission grating. In addition to this, we can easily make them overlapped, in time and space, in a nonlinear medium using the same trick.

In order to obtain a smooth beam profile and the correct beam size, we used a combination of a $\frac{1}{2}$x refractive telescope and a 25μm spatial filter. As a result, the beam size was ~3mm, and the beam profile from the amplifier was improved sufficiently. In order to generate three replicas from the input beam with a smooth intense profile, we use a 2D low density transmission grating where the size of the square dot was 56 μm on one side, and the spacing between the square dots was 102 μmm in Figure 4 – 11. This corresponded to a 9.8-line/mm groove-density for both axes (the vertical and horizontal axes of the grating). In order to separate the beams, sufficient distance (~1.5 m) between the 2D transmission grating and the input mask was required because our 2D grating was

not very dispersive. The same input mask isolated the three first-orders from the pattern, resulting in three replicas of the input beam, as in Figure 4 – 11. As a result, we generate three replicas from the input beam not using beam splitter. In order to make them overlapped, we use a Fresnel biprism and a cylindrical lens like in Figure 4 – 4. Like the simplified TG FROG, two of three replicas were overlapped in space and time at the third-order nonlinear material by a cylindrical lens, producing a line-shaped transient refractive-index grating. The third beam was crossed and delayed by the Fresnel biprism, whose diffraction by the induced grating produced a signal pulse.

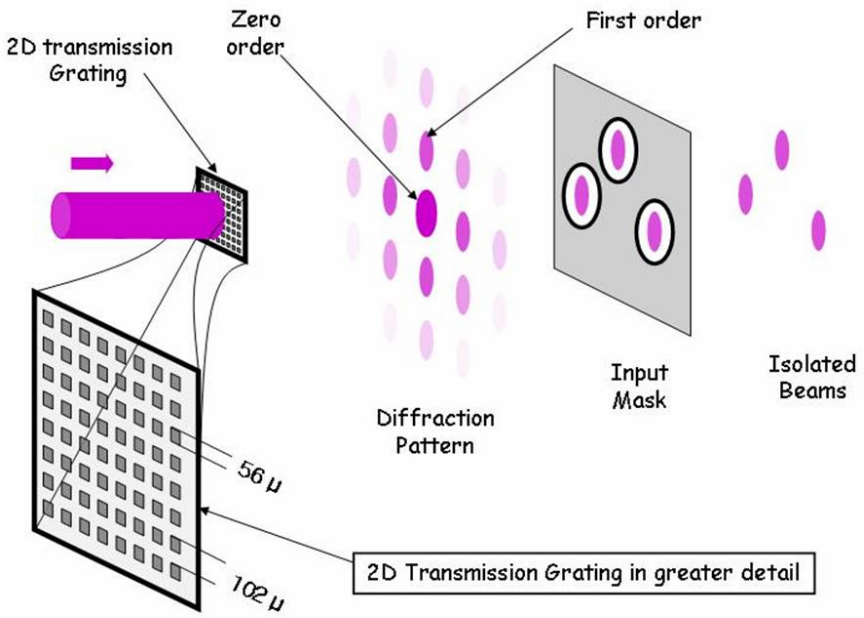

Figure 4 – 11: Diffractive beam splitter and mask for generating the three beams.

4. 6 MEASUREMENTS USING DIFFRACTIVE BEAM SPLITTER

The substrate of the 2D transmission grating was UV-grade fused silica, in which an aluminum coating was applied over a square array. An easily distinguished diffraction pattern formed at a distance (~1.5 m) with a very small angle (~ 0.2°) between the beams. Three first-order beams were transmitted by the input mask. Because the three beams diverged from the 2D transmission grating at a very small angle, they were overlapped just after the focus of the cylindrical lens (Figure 4 – 4), but this effect reduced the intensity at the nonlinear material only slightly.

Using the diffractive beam splitter and mask for generating the three beams, we describe our measurements of 800-nm pulses, which were from a Ti:Sapphire regen and were ~200-fs long, 100μJ in energy, and at 500-kHz-rep-rate. This device also included a simple imaging spectrometer, whose entrance slit comprised the line focus in the glass. The signal was isolated by the output mask and collimated by a spherical lens and diffracted off a 600-line/mm groove-density grating. After a spherical focusing lens, a spectral resolved TG-FROG trace resulted on the CCD camera, in which the delay varied vertically and frequency varied horizontally (Figure 4 – 12). For the third-order nonlinear material, we used a 3mm thick ZnSe [53]. The focal length of the cylindrical lens was 150 mm. The Fresnel biprism had an apex angle of 160°, yielding a delay range of 1.6 ps [54]. The crossing angle of the two pump beams was about 3.8°, resulting in a transient grating with ~ 12 μm spatial period. [56]

The agreement between the measured and retrieved traces (Figure 4 – 13) was very good. The FROG error for the 128×128 traces was about 0.5%. To verify the accuracy of the results, we measured the same pulse, using a commercial GRENOUILLE

from Swamp Optics (Model 8-50). Figure 4 – 13 shows these results, and the agreement is good.

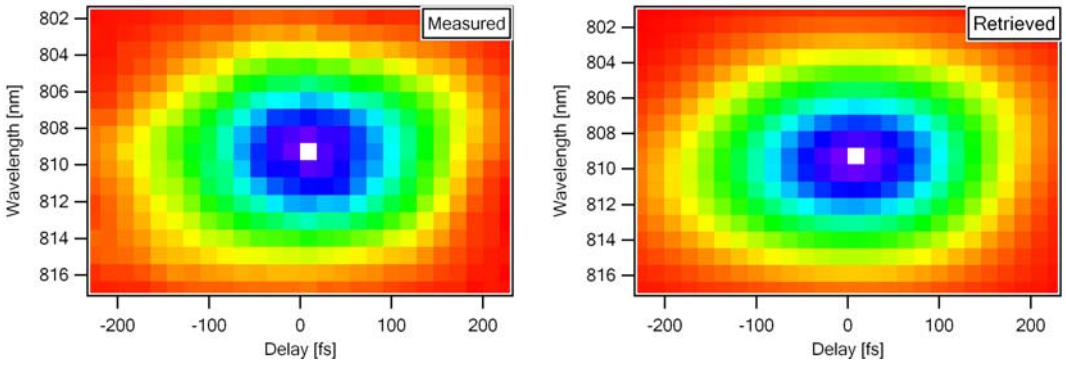

Figure 4 – 12: Measured and retrieved TG FROG traces.

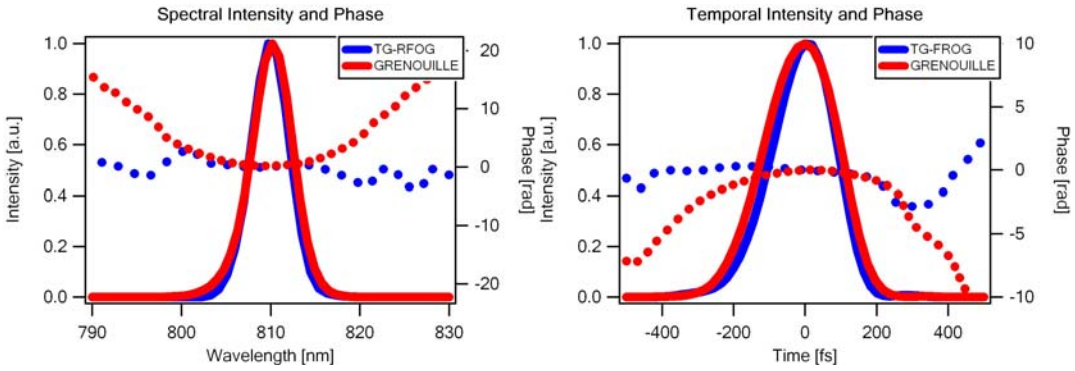

Figure 4 – 13: Retrieved intensity and phase of the pulse using the simplified TG FROG (and GRENOUILLE for comparison). On the left are the spectral intensity and phase; on the right are the temporal intensity and phase.

Consequently, this method, using a 2D transmission grating, has advantages. One of them is that the method can make three replica of the input beam easily without any changes of beam profile. The beams have the Gaussian profile spatially, or Gaussian like profile, if the input beam has the Gaussian profile. Therefore, the center part of the beam, where the beams are overlapped in FROG geometries, is very smooth and strong, and so the energy efficiency of the method is better than the method using input mask. However,

since we use a 2D transmission grating, introducing of the spatial chirp in the beam replicated can not be avoided. If we have pulses with a small bandwidth, it will not be a problem because the spatial chirp introduced from the grating is negligible, pulses with a broad bandwidth starts to introduce the spatial chirp in the replicated pulses seriously. Additionally, the three input beams are not collimated, but they have a diverging angle even though it is very small. Therefore, when the three beams cross and overlap in a nonlinear medium, they do not overlap at their foci but at right after the foci because of the incident angle. Worse, if the center wavelength changes, the diffraction angle will change. As a result, the simplified TG FROG, using 2D transmission grating, is not a broadband pulse- measurement device.

4. 7 CONCLUSIONS

We demonstrated an extremely broadband TG FROG device, which is able to measure amplified pulses over a broad range of wavelengths with no change of components. This device can measure pulses with the center wavelength of 800nm, and without any optics it can measure pulses with the center wavelength of 400nm. Actually, with the same simplified TG FROG device, we measured a pulse with the center wavelength of 276nm, which was a third harmonics of the pulse with 800nm too. In this device, the camera needed to be changed because it required a camera with deep UV responsibility, and we used bi-mirror instead of Fresnel biprism because the pulse was too long to use biprism.

If we had a laser source, which could generate a pulse with high intensity, and with the center wavelength longer than 1000nm, such as 1024nm or 1550nm, the simplified TG FROG device could measure the pulses with a small change such as changing camera or

crystal. As a result, this simplified TG FROG is an extremely broadband device limited only by material transmissivity (in lens or crystal) and camera responsibility.

Also, we believe that this TG FROG device is the best option for UV pulse measurement, in which, before now, we had to use a traditional TG FROG geometry which is most complex with six critical alignment degrees of freedom. Additionally, while OPAs yield weaker pulses in the UV than in the visible and near-IR, third-order nonlinearities increase in the UV, so the device sensitivity scales reasonably.

Finally, while the TG FROG device described here utilizes transmissive components, such as lens and Fresnel biprism. When we have extremely short pulses such as a single-cycle pulse, by changing transmissive components to analogous reflective ones, the device can measure them in order to avoid the material dispersion. For example, the analogous essentially all-reflective simplified TG FROG device uses a bi-mirror, instead of Fresnel biprism, and a cylindrical mirror, instead of a cylindrical lens, like GRENOUILLE did. [58]

CHAPTER 5

CONCLUTIONS AND FUTURE WORKS

It is no doubt that since the first invention of FROG, the SHG FROG has had the inevitable position as the best Ultrafast-laser-pulse measurement device. Actually, the device has been measuring not only a very simple ultrashort pulse such as an almost transform-limited pulse but also a complex pulse such as a single cycle pulse, and the device can measure a pulse with wavelengths, ranging from 600nm to more than 2000nm. With a cross-correlation FROG method, the SHG FROG has been extending its influence over much more complex pulses, like supercontinuum pulses. Besides, after the advent of GRENOUILLE, a simplified SHG FROG, we can in-situ monitor the intensity and phase of our pulse.

However, the ultrashort-laser pulse measurement devices based on the SHG process is limited to wavelengths above the visible light (above 500nm). This device can not measure the UV ultrashort-laser-pulse because the SHG crystal (The shortest wavelength for BBO crystal can be phase-matched 410nm) starts to absorb to SHG at around 200nm. In addition to this, even if it is transparent in near the UV, it is impossible to phase-match the pulse with wavelengths near the UV because we need to use an extremely thin crystal, unable to make before now, in order to phase-match the bandwidth of the pulse. Basically, second-harmonic generation (SHG), the basis of most techniques, has a stringent phase-matching requirement, which limits the use of the devices based on SHG process.

We demonstrate one way to reduce the stringent phase-matching requirement in (cross-correlation) SHG FROG geometry, measuring the supercontinuum from the tapered microstructure fiber. The multi-shot angle-dithering SFG X FROG geometry works very well as long as the pulses we want to measure fulfill the implicit assumption that the intensity and phase of the pulses are the same for each pulse in the measurement. This assumption is acceptable for most of the ulrashort-laser-pulse sources. However, for some of laser sources, like the supercontinuum and a free-electron laser, we fail to accept the assumption.

When we have pulses which fail to fulfill the assumption and have a very broad bandwidth pulse, like the supercontinuum, it is almost impossible to use any pulse measurement device based on SHG process. Worse, like the supercontinuum, the spectra contain the UV or near the UV and the intensity and phase of the pulse is changing shot-to-shot. For measuring the supercontinuum properly, it is necessary to build a FROG geometry which can phase-match a broad bandwidth of the pulse and operate a single-shot. The single-shot TG X FROG is the one which can satisfy all these requirements. We show that this device can measure the continuum from a bulk fused silica, phase-matching the whole bandwidth of the continuum. Right now, it can measure only continuum from fused silica because we need to use relatively high intensity from the continuum source. However, we believe that if the pump beams are strong enough to gate a weak pulse, the supercontinuum from microstructure fibers can be measured using the single-shot TG X FROG geometry.

One big issue for TG FROG is complexity due to using a three-beam geometry, even though TG FROG geometry is the most versatile, sensitive, and accurate. Here we

demonstrate an ultrasimple extremely broadband TG FROG, removing complexities of the inherent TG FROG geometry. Using this device, we measure not only the ultrashort-laser-pulse centered at 800nm but also the UV ultrashort-laser-pulse without any change of optics. We believe that this device plays a key role to characterize the UV ultrashort-laser-pulse, which can not be measured by GRENOUILLE based on SHG process.

Another issue for TG FROG is that this geometry requires high intensity pulses. We use a ZnS crystal or a ZnSe crystal as a third-nonlinear medium which has a relatively high third-nonlinear optical coefficient in order to generate enough signal strength with relatively low intensity pulses. However, in these days, many high power ultrashort-laser sources, such as a CPA regenerative amplifier system, many research groups have, are accessible, and the pulses from the sources need to be characterized. Therefore, we believe that TG FROG, which is the most sensitive version among the FROG geometries using the third-nonlinear process, is extending its influence.

One of the ultrafast-laser scientists' goals is making the pulses shorter and another is making the intensity of the pulses higher. We believe that in order to measure the short pulses with an extremely broad bandwidth, we need to use a TG FROG geometry which can phase-match the whole bandwidth simultaneously. In addition to this, one way to make a very short pulse is compressing the supercontinuum. To do this, we need to measure the supercontinuum properly (and in-situ). We can suggest that TG X FROG geometry is the best option for doing the compression from the supercontinuum.

REFERENCES

[1] K. DeLong, D. Fittinghoff, and R. Trebino, “Practical issues in ultrashort-laser-pulse measurement using frequency-resolved optical gating," IEEE J. Quant. Electron, 32, pp. 1253, 1996.

[2] K. DeLong, D. Fittinghoff, R. Trebino, A. Sullivan, J. Hunter, W. White, and D. Kane, “Frequency-resolved optical gating: Measuring the intensity and phase of an ultrashort laser pulse," in Ultrafast Phenomena IX (Barbara, P., Knox, W., Mourou, G., and Zewail, A., eds.), Springer Series in Chemical Physics,127, Berlin: Springer-Verlag, 1994.

[3] K. DeLong, R. Trebino, J. Hunter, and W. White, “Frequency-resolved optical gating with the use of second-harmonic generation," J. Opt. Soc. Amer. B, 11, 2206, 1994.

[4] L. Cohen, “Time-Frequency Distributions- A review. Proceedings of IEEE, Vol 77, pp. 194, 1989.

[5] L. Cohen, “Time-Frequency Analysis” Englewood Cliffs, NJ: prentice-Hall.

[6] S. Akturk, M. Kimmel, P. O'Shea, and R. Trebino, “Extremely simple device for measuring 20-fs pulses” Optics Letters, Vol. 29, Issue 9, pp. 1025-1027, 2004.

[7] S. Akturk, M. Kimmel, R. Trebino, S. Naumov, E, Sorokin, and I. Sorokina, “Measuring several-cycle 1.5-m pulses using frequency-resolved optical gating ” Optics Express, Vol. 11, Issue 25, pp. 3461-3466 (December 2003).

[8] P. O'Shea, M. Kimmel, X. Gu, and R. Trebino,” Highly simplified device for ultrashort-pulse measurement,” Optics Letters, Vol. 26, Issue 12, pp. 932-934 (2002).

[9] H. Stark, ed. “Image Recovery: Theory and Application,” Academic Press 1987.

[10] M. Maier, W. Kaiser, and J. A. Giordmaine, Phys. Rev. Lett., 1966. 17:pp. 1275.

[11] V. V. Kotlyar, P. G. Seraphimovich, and V. A. Soifer, “Regularized Iteraative Algorithm for the Phase Retrieval,” Optik, 94, pp. 96, 1993.

[12] J. R. Fienup, “Phase Retrieval Algorithms: A Comparison,” Applied Optics, 21, pp. 2758, 1982.

[13] D. Peri, “Optical Implementation of a Phase Retrieval Algorithm,” Applied Optics, 26,pp.1782, 1987.

[14] K. W. DeLong, D. N. Fittinghoff, R. Trebino, B. Kohler, and K. Wilson, "Pulse Retrieval in Frequency-Resolved Optical Gating Based on the Method of Generalized Projections," Optics Letters, 19, pp. 2152, 1944.

[15] A. Levi, H. Stark, "Restoration from Phase and Magnitude by Generalized Projections," in imaging Recovery: Theory and Application, ed. Academic, 1987.

[16] E. Yudilevich, A. Levi, G. J. Habetler, and H. Stark, "Restoration of signals from their signed Fourier-transformation magnitude by the method of generalized projections," J. Opt. Soc. Amer. A, 4, pp.236 1987.

[17] C. Iaconis, and I. A. Walmsley, "Spectral Phase Interferometry for direct electric-field Reconstruction of ultrashort optical pulses," Optics Lett., 23, pp.972, 1998.

[18] D. J. Kane, and R. Trebino, "Single-shot Measurement of the intensity and Phase of an Arbitrary Ultrashort Pulse By Using Requency-Resolved Optical Gating," Opt. Lett., 18, pp. 823, 1993

[19] T. S. Clement, A. J. Taylor, and D. J. Kane, "Sinlge-Shot measurement of the amplitude and Phase of ultrashort laser pulses in the violet," Optics Lett., 20, pp.70, 1995.

[20] J. N. Sweetser, D. N. Fittinghoff, and R. Trebino, "Transient-Grating Frequency-Resolved Optical Gating," Optics Letters, 22, pp. 519, 1997.

[21] S. A. Arakelian, R. N. Gyuzalian, and S. B. Sogomonian, "Comments on the Picosecond Pulse Width Measurement by the Single-shot Second Harmonic Beam Technique," Optics Communications, 44, pp. 67, 1982.

[22] J. Ranka, R. Windeler, and A. J. Stentz, "Visible continuum generation in air-silica microstructure optical fibers with anomalous dispersion at 800nm", Optics Letters. 25, pp.25, 2000

[23] W. J. Wadsworth, A. Ortigosa-Blanch, J. C. Knight, T. A. Birks, T. P. M. Man, and P. St. J. Russell, J. Opt. Soc. Am. B 19, 2148, 2002.

[24] I. Hartl, X. D. Li, C. Chudoba, R.K. Ghanta, T. H. Ko, J. G. Fujimoto, J. K. Ranka, and R. S. Windeler, Optics Letters, 26, pp. 608, 2001.

[25] S. A. Diddams, D. J. Jones, J. Ye, S. T. Cundiff, J. L. Hall, J. K. Ranka, R. S. Windeler, R. Holzwarth, T. Udem, and T. Hansch, Phys. Rev. Letters, 84, pp. 5102, 2000.

[26] F. Quochi,M.Dinu, L. N. Pfeiffer, K. W. West, C. Kerbage, R. S. Windeler, and B. J. Eggleton, Phys. Rev. B 67, pp. 235323, 2003.

[27] A.V. Husakou, J. Herrmann, Phys. Rev. Letters, 87, pp. 203901, 2001.

[28] A.L. Gaeta, "Nonlinear propagation and continuum generation in microstructured optical fibers," Opt. Letters, 27, pp. 924, 2002.

[29] J. M. Dudley, S. Coen, "Coherence properties of supercontinuum spectra generated in photonic crystal and tapered optical fibers," Opt. Letters, 27, 1180, 2002.

[30] D. Akimov, M. Schmitt, R. Maksimenka, K. Dukel'skii, Y. Kondrat'ev, A. Khokhlov, V. Shevandin, W. Kiefer, and A. Zheltikov, Appl. Phys. B 77, pp. 299, 2003.

[31] L.M. Tong, R.R. Gattass, J.B. Ashcom, S.L. He, J. Y. Lou, M. Y. Shen, I. Maxwell, and E. Mazur, Nature 426, pp. 816, 2003.

[32] A. M. Zheltikov, Optics and Spectroscopy, 95, pp. 410, 2003.

[33] L. M. Tong, J. Y. Lou, and E. Mazur, "Investigation and optimization of bidirectionally dual-order pumped distributed Raman amplifiers," Opt. Express, 12, pp. 1025, 2004.

[34] M. A. Foster, K. D. Moll, and A. L. Gaeta, "Optimal waveguide dimensions for nonlinear interactions," Opt. Express, 12, pp. 2880, 2004.

[35] M.A. Foster, and A.L. Gaeta, "Ultra-low threshold supercontinuum generation in sub-wavelength waveguides,"Opt. Express, 12, pp. 3137, 2004.

[36] M. Kolesik, E. Wright, J. Moloney, Appl. Phys. B 79, pp. 293, 2004.

[37] S. Leon-Saval, T. Birks, W. Wadsworth, P. Russell, and M. Mason, "Supercontinuum generation in submicron fibre waveguides," Opt. Express, 12, pp. 2864, 2004.

[38] J. Knight, J. Arriaga, T. Birks, A. Ortigosa-Blanch, W. Wadsworth, and P. Russell, IEEE Photon. Technol. Letters, 12, pp. 807, 2000.

[39] V. Finazzi, T.M. Monro, and D.J. Richardson, IEEE Photon. Technol. Letters, 15, pp. 1246, 2003.

[40] E.C. Magi, H.C. Nguyen, and B. J. Eggleton, "Air-hole collapse and mode transitions in microstructured fiber photonic wires," Opt. Express, 13, pp. 453, 2005.

[41] T.A. Birks, and Y.W. Li, J. Lightwave Technol., 10, pp. 432, 1992.

[42] J.M. Dudley, X. Gu, L.Xu, M. Kimmel, E. Zeek, P. O'Shea, R. Trebino, S. Coen, and R.S. Windeler, "Cross-correlation frequency resolved optical gating analysis of broadband continuum generation in photonic crystal fiber: simulations and experiments "Opt. Express, 10, pp. 1215, 2002.

[43] J. H. V. Price, W. Belardi, T. M. Monro, A. Malinowski, A. Piper, D. J. Richardson, "Soliton transmission and supercontinuum generation in holey fiber using a diode pumped Ytterbium fiber source," Opt. Express 10, 382– 387 (2002)

[44] J. M. Dudley, "supercontinuum generation in photonic crystal fiber", Reviews of modern physics 78, 1135-1184 2006)

[45] R. R. Alfano, ed., "The Supercontinuum Laser Source" (Springer-Verlag, New York, 1989).

[46] K. R. Wilson and V. V. Yakovlev, J. Opt. Soc. Am. B 14, 444 (1997).

[47] X. Gu, L. Xu, M. Kimmel, E. Zeek, P. O'Shea, A. P. Shreenath, R. Trebino, and R. S. Windeler, "Frequency-resolved optical gating and single-shot spectral measurements reveal fine structure in microstructure-fiber continuum", Opt. Lett. 27, 1174-1176.

[48] J. N. Sweetser, D. N. Fittinghoff, and R. Trebino, "Transient-Grating frequency-resolved optical gating" Optics Lett., vol. 22, 519-521 (1997).

[49] Eckbreth, A.C., BOXCARS: Crossed Beam Phase-matched CARS generation in Gases. Appl. Phys. Lett., 1978. 32(7): 421-3.

[50] J. B. Ashcom, R. R. Gattass, C. B. Schaffer, and E. Mazur, "Numerical aperture dependence of damage and supercontinuum generation from femtosecond laser pulses in bulk fused silica", J. Opt. Soc. Am. B 23 2317 (2006).

[51] R. Trebino, "Frequency-Resolved Optical Gating: The Measurement of Ultrashort Laser Pulses", Chapters 6, 7 (Kluwer Academic Publishers, 2002).

[52] Brodeur, A., and S. L. Chin, 1998, "Band-gap dependence of the ultrafast white-light continuum," Phys. Rev. Lett. 80, 4406–4409.

[53] R. Trebino, K. W. DeLong, D. N. Fittinghoff, J. N. Sweetser, M. A. Krumbugel, B. A. Richman, and D, J, Kane, "Measuring ultrashort laser pulses in the time frequency domain using frequency-resolved optical gating," Review of Scientific Instruments, 68, pp. 3277, 1997.

[54] R. Trebino, Frequency-Resolved Optical Gating: The Measurement of Ultrashort Laser Pulses (Kluwer Academic Publishers, 2002).

[55] M. Li, J. P. Nibarger, C. Guo, and G. N. Gibson, "Dispersion-free Transient-Grating frequency-resolved optical gating" Applied Optics, 38, pp. 5250, 1999.

[56] H. J. Eichler, P. Gűnter, and D. W. Pohl, Laser-Induced Dynamic Gratings (Springer-Verlag Berlin Heidelberg, 1986).

[57] R. W. Boyd, Nonlinear Optics (Academic Press, 2003), Chapter 4.

[58] S. Akturk, M. Kimmel, P. O'Shea, R. Trebino," Extremely simple device for measuring 20-fs pulses" Optics Letters, 29, pp. 1025, 2004.

VITA

Dongjoo Lee

Dongjoo Lee was born in Seoul, South Korea, on January 15th 1967. He graduated from Sogang University, Seoul, Korea, with a degree of B.S. and from Seoul National University, Seoul, Korea, with a degree of MS in Physic. After his M.S., he had worked for Samsung Electronics for about 5 years. In this company, he was working as a senior engineer in the manufacturing technology team, in the Semiconductor research group of Samsung Electronics. From 2002, he is pursuing his PhD studies in the field of Ultrafast Optics, in the research group of Rick Trebino at School of Physics, at Georgia Institute of Technology. When he is not working on his research, Dongjoo Lee enjoys going fishing to Florida beach with his son, Seungmin, and his wife, Seonghee Jeong. Also, he likes playing most of sports, like tennis, ping-pong, swimming, and golf.